Combined effects of urban morphology on land surface temperature and PM$_{2.5}$ concentration across fine-scale urban blocks in Hangzhou, China

Xin Chen , Fang Wei [*]

College of Civil Engineering and Architecture, Zhejiang University, Hangzhou 310058, China

A B S T R A C T

Optimizing urban morphology can effectively mitigate high land surface temperature (LST) in summer and PM$_{2.5}$ pollution in winter. However, the lack of high-resolution PM$_{2.5}$ data hinders the study across all fine-scale blocks within the urban area. Additionally, the complexity of the thermal and atmospheric environments necessitates an in-depth analysis of the combined effects of urban morphology. This study takes the central urban area of Hangzhou as the study area, identifying urban blocks within it as study units. Urban morphology metrics, average LST (derived from remote sensing inversion), and average PM$_{2.5}$ concentrations (downscaled using the land use regression model) are calculated for each block. Furthermore, the nonlinear regression model and bootstrapping mediation analysis are applied to examine the nonlinear effects and mediating mechanisms of urban morphology on summer LST and winter PM$_{2.5}$. The findings show that (1) most urban morphology metrics exhibit nonlinear relationships with LST and PM$_{2.5}$, except for the correlations between LST and floor area ratio, and between LST and spatial congestion degree. However, the morphological metrics for most blocks did not exceed the threshold, leading to the unidirectional total effect. (2) In winter, LST plays a significant role in mediating the effect of urban morphology on PM$_{2.5}$, with the proportion mediated exceeding 9.0%. In contrast, the mediation of urban morphology on LST by PM$_{2.5}$ is relatively minimal in summer, with the proportion mediated remaining below 2.2%. (3) Mid- to high-rise, low-density building mode can alleviate high LST and PM$_{2.5}$ concentration, particularly in waterfront urban blocks with high-intensity development.

1. Introduction

Rapid urbanization has replaced natural landscapes with impervious surfaces, accommodating large influxes of people from rural areas [1,2]. Simultaneously, numerous buildings are constructed to support thriving human production and living activities [3]. While this drives significant socio-economic prosperity, it also poses environmental threats [4,5]. In particular, the disorderly urban expansion and dense building distributions have intensified industrial production, exacerbated excessive energy consumption [6,7], and restricted atmospheric circulation within cities and between urban and suburban areas [8,9]. Consequently, large quantities of air pollutants, greenhouse gases, and heat are emitted without adequate capture or dissipation, severely damaging both atmospheric and thermal environments [5,10]. In recent years, heatwaves during summer and PM$_{2.5}$ in winter have emerged as two critical challenges confronting large cities globally [11,12]. Land surface temperature (LST) is recognized as a key factor of heatwave threats [13,14], and its ease of monitoring has led to its widespread use in research [11,15,

16]. Both high LST and PM$_{2.5}$ concentrations can disrupt ecosystems, harm public health, and subsequently affect social development [5,17, 18]. Therefore, to mitigate these pressing issues, it is imperative to reconsider and redesign urban spatial patterns.

Urban blocks represent the fundamental units of the urban physical environment and serve as the direct focus for implementing urban policy and planning initiatives [19,20]. Urban morphology acts as an effective lever for block planning [21,22], primarily manifesting in the spatial configuration of buildings at the block level [23,24]. Urban morphology influences local microclimates [25,26], surface energy balance [27], and human behavior [28], thereby comprehensively affecting both atmospheric and thermal environments. Furthermore, a complex interplay exists between LST and PM$_{2.5}$ [29,30]. PM$_{2.5}$ affects the ground's reception of shortwave and longwave radiation in opposing ways, thereby influencing LST [31]. Meanwhile, LST affects turbulence and the height of the mixing layer, which in turn influences PM$_{2.5}$ concentrations [32]. Therefore, optimizing urban spatial patterns to mitigate PM$_{2.5}$ pollution and high LST requires addressing the critical scientific

---

question: How does urban morphology at the block level directly influence LST and $PM_{2.5}$ concentrations, and does a mediating process exist whereby urban morphology affects $PM_{2.5}$ through LST, or vice versa?

Existing studies have widely identified the direct linear effects of urban morphology on LST and $PM_{2.5}$. For example, higher-density building layouts typically hinder atmospheric circulation, thereby increasing $PM_{2.5}$ concentrations [33,34] and elevating LST [35,36]. Greater average building height can promote air circulation to disperse pollutants and heat, which often negatively correlates with $PM_{2.5}$ concentrations [37]. However, taller buildings can also block solar radiation, leading to an uncertain relationship with LST [36,38,39]. A larger sky view factor indicates more open space, which helps reduce $PM_{2.5}$ concentrations [33,40]. However, it also lowers the blocking of solar and ground radiation, resulting in a rise in LST [41,42]. Meanwhile, few studies have focused on the potential mediating mechanisms linking urban morphology, LST, and $PM_{2.5}$. For example, Liang et al. found that a larger fractal dimension of urban space increases $PM_{2.5}$ concentrations, further exacerbating the nighttime urban heat island effect [43]. Cao et al. found that in winter, the proportion of urban forest areas can reduce regional $PM_{2.5}$ concentrations, but this effect is partially suppressed by the indirect influence of urban forest areas on LST [44]. Given the complexity of the interactions between urban morphology, LST, and $PM_{2.5}$, more research is needed to further explore the nonlinear effects of urban morphology on $PM_{2.5}$ and LST, as well as the potential mediating mechanisms through which urban morphology influences LST and $PM_{2.5}$.

Furthermore, due to the resolution limitations of available $PM_{2.5}$ data, combined research of $PM_{2.5}$ and LST at high-resolution (<1 km) across all fine-scale blocks within the urban area is constrained. Specifically, previous studies typically relied on remote sensing imagery to retrieve LST, with data resolutions as high as 30 m, enabling comprehensive analysis of fine-scale urban blocks [24,35,45]. Additionally, open-source air quality datasets based on remote sensing provide global $PM_{2.5}$ concentration estimates, which are widely used for city-wide research [44,46]. However, these datasets are limited to a maximum resolution of 1 km, which remains too coarse for fine-scale blocks [24]. In contrast, simulation modeling and station-based/mobile monitoring equipment can achieve $PM_{2.5}$ concentration data at resolutions below 1 km [47,48]. Nevertheless, the high costs and operational complexities associated with these methods restrict their applicability to large urban areas. As a result, such studies are often confined to specific individual blocks within cities [33,34]. Therefore, research on thermal and atmospheric environments across all fine-scale blocks within the urban area requires breakthroughs in $PM_{2.5}$ data.

To address these research gaps, new approaches grounded in existing methodologies need to be explored. (1) The land use regression (LUR) model, originally developed for epidemiological studies, provides an effective framework for estimating fine-scale pollutant concentrations [49,50]. The LUR model constructs a fitting equation based on pollutant concentrations from air quality monitoring stations and related variables (such as land use and socio-economic status) within surrounding buffer zones, thereby generating air pollutant concentration maps for a region [51,52]. In this study, we extract $PM_{2.5}$ concentration raster data and convert it to point-level data, which is then used as the dependent variable for LUR regression. This approach could substantially enable the downscaling of $PM_{2.5}$ data [53]. (2) Nonlinear regression model (NRM) [54] and bootstrapping mediation analysis [55] in econometrics can be applied to investigate the combined effects of urban morphology on the thermal and atmospheric environments. Compared to meteorological models based on physical mechanisms, these methods offer a simpler and more cost-effective way to capture the correlations between variables. Furthermore, unlike data-driven machine learning models, NRM and mediation analysis allow for specifying and testing causal mechanisms between variables, providing potential explanatory insights into the underlying processes.

Hangzhou, the capital city of Zhejiang Province in China, is characterized by rapid socio-economic development, diverse urban block morphology designs, and significant thermal and atmospheric environmental challenges. This study identifies urban blocks within the core urban area of Hangzhou as the study units and calculates their urban morphology metrics. LST inverted from remote sensing images and $PM_{2.5}$ concentrations downscaled by the LUR model are averaged within blocks for both summer and winter. Furthermore, the direct nonlinear effects and indirect mediating mechanisms of urban morphology on LST in summer and $PM_{2.5}$ in winter are analyzed. The main objectives of this study are as follows: (1) Mapping and analyzing the LST and $PM_{2.5}$ situations across all fine-scale urban blocks within the city; (2) Applying NRM and mediating analysis to thoroughly analyze the direct nonlinear and indirect mediating effects of urban morphology on the LST and $PM_{2.5}$; (3) Proposing potential urban planning and block morphology optimization strategies. The subsequent sections are organized as follows: Section 2 provides a detailed description of the study area, period, and data; Section 3 introduces the methods applied in the study; Section 4 presents the research results; Section 5 offers an in-depth discussion of the methodology, results, and limitations; and Section 6 concludes with the research findings.

2. Materials

2.1. Study area and period

Hangzhou, the capital of Zhejiang Province within the Yangtze River Delta urban agglomeration in southeastern China [56], is administratively divided into 13 counties (Fig. 1). This study focuses on the four counties comprising the core urban area of Hangzhou: Shangcheng, Gongshu, Xihu, and Binjiang. These counties were selected for the following reasons: (1) the area is a typical representative of Hangzhou's socio-economic prosperity, accounting for 46.5% of the city's GDP and 34.5% of its resident population in 2022. (2) The region primarily consists of densely built-up urban areas with diverse urban morphology, while still featuring some surrounding forests and water bodies, forming a relatively complete land-use structure. (3) Rapid urbanization in the area has led to deteriorating thermal and atmospheric environments, with urban heatwave and haze pollution frequently occurring in recent years [57,58]. Furthermore, urban blocks are selected as the basic study units. Urban blocks must meet two criteria: (1) being delineated by man-made or natural boundaries, and (2) primarily consisting of urban space.

This study selects the summer (June) and winter (January) of 2023 as study periods. The reasons are as follows: (1) between 2019 and 2022, the COVID-19 pandemic significantly impacted human activities, leading to unnatural fluctuations in the atmospheric environment. These disruptions could compromise the validity of the study's results. Additionally, obtaining urban morphology data before 2019 is challenging, and its relevance has diminished over time. (2) Summer and winter are the peak seasons for urban heatwave and haze pollution, respectively. For this study, the optimal remote sensing images for retrieving LST in Hangzhou were captured in late May (considered as June for summer) and January (for winter) of 2023.

2.2. Data description

The data used in this study are presented in Table 1. Remote sensing data were used to retrieve LST. $PM_{2.5}$ concentration data, as raw data, were downscaled using the LUR model. Road network data were used to identify urban blocks. Building data, including height attributes, was used to calculate the urban morphology within the blocks. Land use data were used in two ways: (1) to extract boundaries for mountains and water bodies to identify the urban blocks, and (2) alongside point of interest (POI) data, nighttime light (NTL) data, population density data, non-$PM_{2.5}$ air pollutant data, and meteorological data to form the
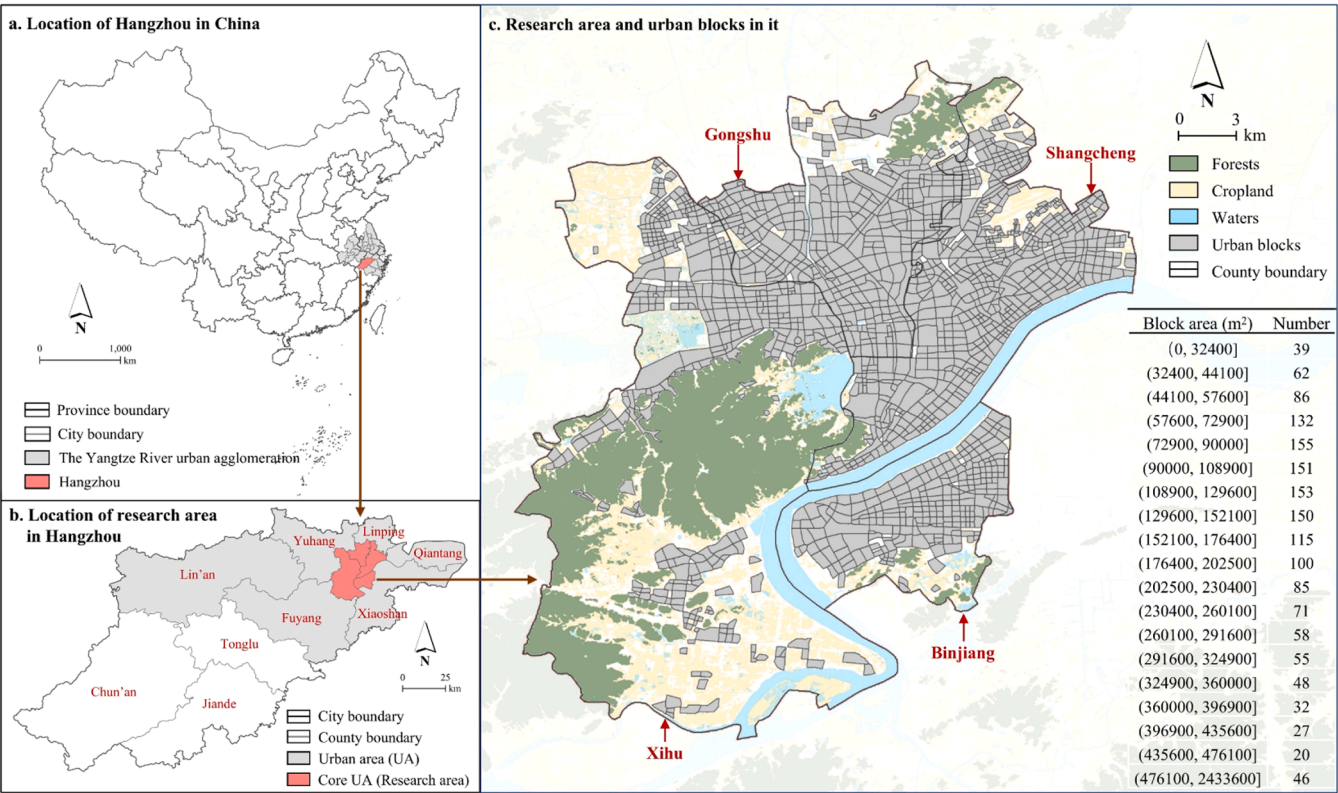
Fig. 1. Location of research area and urban blocks in it.

Table 1

Data used in the study and their description.

Data type	Dataset name	Time	Resolution	Source
Remote sensing data	Landsat 8 Level 2, Collection 2, Tier 1	2023.01.20 (02:31:53);2023.05.28 (02:30:53)	30 m	http://earthexplorer.usgs.gov/
PM$_{2.5}$ data	ChinaHighPM$_{2.5}$	2023.01; 2023.06	1000 m	http://data.tpdc.ac.cn/
Road network data	–	2023	–	https://www.openstreetmap.org/
Building data	Building height of Asia in 3D-GloBFP	2020	–	https://zenodo.org/records/11397015
Land use data	China Land Cover Dataset (CLCD)	2023	30 m	https://zenodo.org/records/12779975
POI data	–	2023	–	https://ditu.amap.com/
Population data	Landscan High Definition (HD)	2022	100 m	https://landscan.ornl.gov
NTL data	VIIRS Nighttime lights (VNL)	2023.01; 2023.06	500 m (resampled to 100 m)	https://payneinstitute.mines.edu/eog/
Air pollutants data (except PM$_{2.5}$)	ChinaHighAirPollutants (SO$_2$, PM$_{10}$, NO, O$_3$, CO)	2023.01; 2023.06	1000 m (resampled to 100 m)	http://data.tpdc.ac.cn/
Meteorological data	1-km monthly mean temperature/ precipitation dataset for China	2023.01; 2023.06	1000 m (resampled to 100 m)	http://data.tpdc.ac.cn/
District boundary data	–	2023	–	https://www.resdc.cn/

independent variables in the LUR model. Administrative boundary data were used to extract portions of the datasets within the study area.

To meet the requirements of the study period, data with significant seasonality, such as air pollutant concentrations and meteorological data, were averaged for January and June based on their daily average values. The remote sensing image from January 20th (with 0.33% cloud cover) was selected for the January data. However, all June images had cloud cover exceeding 10%, which occluded the study area and reduced data quality. Therefore, the image from May 28th (with 0.87% cloud cover) was selected as a substitute for the June data. Additionally, road network, land use, and POI data are relatively stable across seasons, so the 2023 annual data were used. Given the data availability limitations, and considering that buildings and population in a specific area tend to

remain relatively stable over a period, 2020 building data and 2022 population density data were used as substitutes.

To meet the requirement for fine-scale units, the precision of all data was controlled to be 100 meters or less. Due to data availability limitations, the original precision of air pollutant concentration and meteorological data was 1 km, while nighttime light data had a resolution of 500 meters. Among these, PM$_{2.5}$ concentration is the target for downscaling and is the dependent variable in the LUR model. The other data are used as independent variables in the LUR model fitting, thereby their resolution was improved to 100 meters through cubic convolution reclassification to ensure data consistency. Resampling and scaling of the independent variables in the fitting model have been confirmed as reliable in existing research [59,60].

3. Methodology

The research framework of this study is illustrated in Fig. 2. The main steps include: (1) urban blocks are identified as the research units within the core urban area of Hangzhou using road network, land use, and district boundary data in ArcGIS. Urban morphology metrics for each block are calculated based on building data. (2) LST is inverted using remote sensing image data in ENVI and spatially joined to urban blocks in ArcGIS. Additionally, regression variables are extracted in ArcGIS, and the LUR model is constructed in Python to downscale $PM_{2.5}$ concentration data, which is then spatially allocated to urban blocks in ArcGIS. (3) The NRM is constructed in Python and the bootstrapping mediation analysis is conducted in SPSS to explore the combined effects of urban morphology on LST in summer and $PM_{2.5}$ in winter.

3.1. Block identification and urban morphological metrics

We define urban blocks for the study as spatial units delineated by urban roads, rivers, and mountainous areas. The specific steps for block identification are as follows: (1) human-made boundaries are selected from the road network data, including railways, highways, primary roads, and secondary roads. The centerlines of these roads are then extracted. (2) Natural boundaries, such as mountains (with an elevation difference greater than 50 m) and rivers (with a width greater than 30 m), are extracted from the land use data. Boundaries adjacent to roads (where the average distance to parallel roads is less than 100 m) are removed. (3) Cartographic checks are performed by overlaying the road

centerlines with the boundaries of mountains and rivers. This includes removing disconnected lines and completing unconnected lines. The boundaries are then manually calibrated based on remote sensing imagery. (4) Using the boundary lines obtained in the previous steps, the study area is divided into different blocks. The proportion of impervious surfaces and building density in each block is calculated. Blocks are defined as research objects if the impervious surface ratio exceeds 50% and the building density exceeds 10%. A total of 1585 fine-scale urban blocks were identified (Fig. 1). The median area of the blocks is 131311.2 m^2 (approximately 360^2), with around 40% of the blocks having areas ranging from 72900 (270^2) m^2 to 152100 (390^2) m^2. Therefore, to both assess the pollution status of the blocks and simplify the operational load, the target resolution for downscaling $PM_{2.5}$ concentration data was set at 360 m.

Furthermore, urban morphological metrics for each block were calculated. The selection of urban morphological metrics in this study was based on the following criteria: (1) metrics that are easy to calculate and can be directly applied in planning practice. (2) Metrics that have been validated to be sufficiently representative of multi-dimensional urban morphology and exhibit a clear correlation with the urban thermal and atmospheric environments in related studies. (3) Streamlined and effective metrics that avoid redundant indicators with similar representational meanings. Based on relevant studies [57,36,37], six metrics were ultimately selected. These metrics reflect the one-dimensional, two-dimensional, and three-dimensional urban morphology at the block scale, as detailed in Table 2.
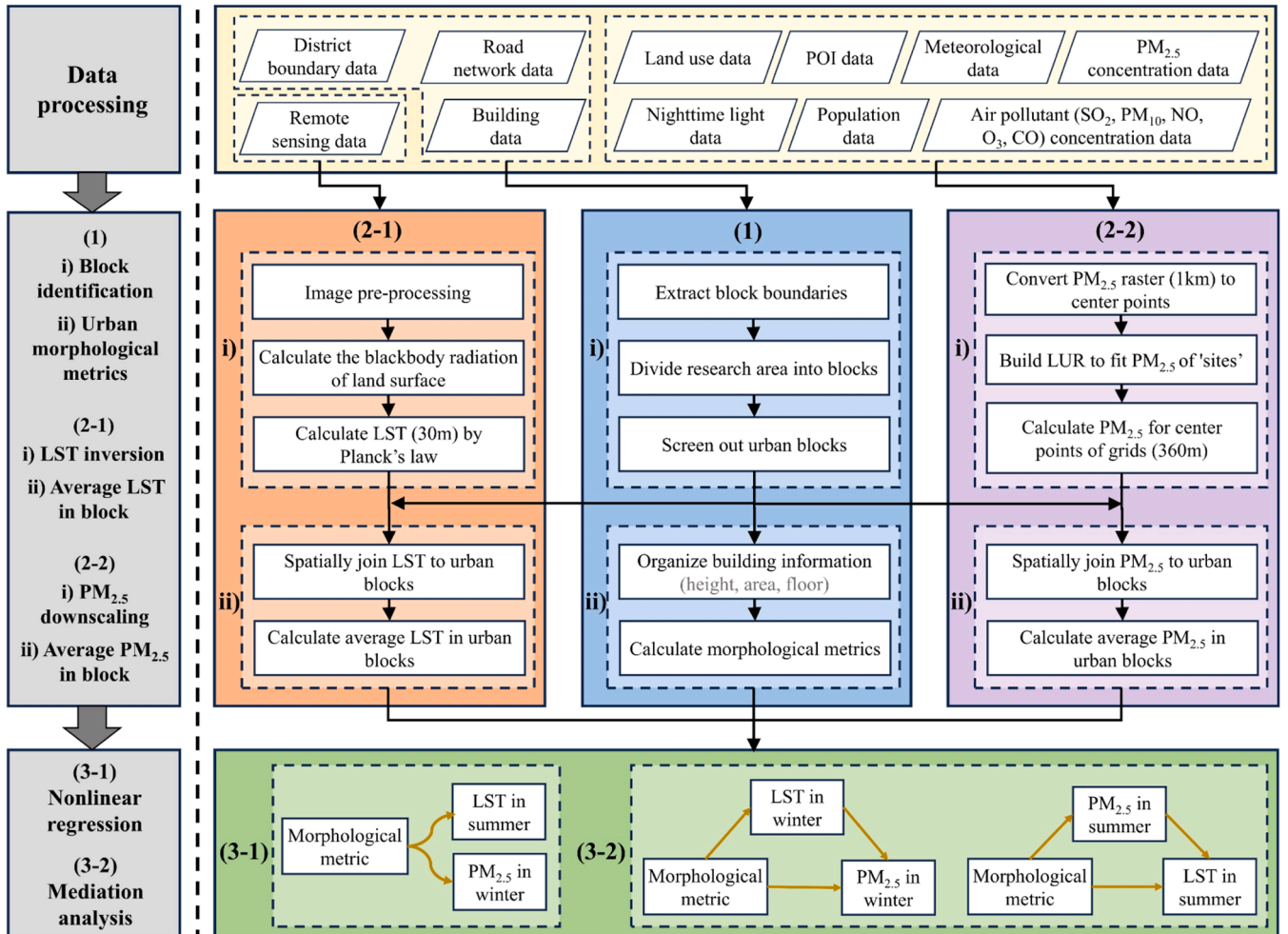

Fig. 2. Research framework.

Table 2
Urban morphological metrics selected in the study.

Dimensionality	Metrics (Acronym)	Formula and description	Significance
One-dimensional height	Average building height (ABH)	$ABH = \sum_{i=1}^{n} H_i / n$ H_i represents the height of building i; n represents number of buildings in the calculated block.	Reflecting the average level of building height in the block.
	Standard deviation of building height (SDBH)	$SDBH = \sum_{i=1}^{n} (H_i - \overline{H})^2 / n$ H_i represents the height of building i; $\overline{H}$, n respectively represents average building height and number of buildings in the calculated block.	Reflecting dramatic changes in building height in the block.
Two-dimensional plane	Building density (BD)	$BD = \sum_{i=1}^{n} A_i / S$ A_i represents the base area of building i; S represents the area of the calculated block.	Reflecting the proportion of building footprints within the area of the block.
	Floor area ratio (FAR)	$FAR = \sum_{i=1}^{n} A_i f_i / S$ A_i, f_i respectively represents the base area and number of floors of building i; S represents the area of the calculated block.	Reflecting the intensity of land development, higher values mean more intensity.
Three-dimensional space	Sky view factor (SVF)	$SVF = 1 - \frac{\sum_{i=1}^{n} \sin\gamma_i}{n}$ γ_i represents the influence of the terrain height angle of buildings on the azimuth angle i; n is the number of calculated azimuth angles.	Reflecting the degree of obstruction of viewpoints by surrounding buildings.
	Spatial congestion degree (SCD)	$SCD = \sum_{i=1}^{n} A_i H_i / (S * H_{max})$ A_i, H_i respectively represents the base area and height of building i; S represents the area of the calculated block; H_{max} represents the max height of buildings within the calculated block.	Reflecting the degree of congestion of buildings in three-dimensional space within the block.

Note: SVF is first calculated in grids of 100*100 m, then the SVF of each urban block is the average of SVFs of grids within the urban block.

3.2. LST inversion

The radiative transfer equation (RTE) method is an effective approach for inverting LST from remote sensing imagery and has been widely applied in related studies [61,62]. The basic principle of the RTE is as follows: (1) the thermal infrared radiation (Eq. (1)) received by remote sensing imagery includes the direct radiation from the atmosphere above the surface (upward radiation), the reflected radiation from the atmosphere above the surface (downward radiation), and the radiation emitted by the surface itself [63]. (2) The radiated energy emitted by any material surface is directly related to its temperature [64], and this relationship follows Planck's law. Therefore, by isolating the surface radiative energy from the thermal infrared radiation (Eq. (2)) in remote sensing imagery, the LST can be further calculated using Planck's equation (Eq. (3)). The formulas are as follows:

$$L_{obs} = (L_T \in + L_d(1 - \in))\tau + L_u \tag{1}$$

$$L_T = \frac{(L_{obs} - L_u - \tau(1 - \in)L_d)}{\in \tau} \tag{2}$$

$$LST = \frac{K_2}{\ln\left(\frac{K_1}{L_T} + 1\right)} - 273.15 \tag{3}$$

In Eq. (1) and Eq. (2), L_T represents the blackbody radiance emitted by the surface that needs to be calculated; L_{obs}, L_u, and L_d represent the total radiance received by the satellite sensor, upward radiation, and downward radiation, respectively, all of which can be directly retrieved from the remote sensing imagery spectral bands. $\in$ and τ represent the emissivity and atmospheric transmittance, respectively, and can also be directly obtained from the spectral band information of the remote sensing imagery. In Eq. (3), LST represents the land surface temperature to be calculated, K_1 and K_2 represent the calibration coefficients for the 10th band of the remote sensing imagery, with values of 774.8853 and 1321.0789, respectively.

3.3. PM$_{2.5}$ downscaling based on LUR model

Based on the fundamental principles and practical experience of the LUR model [51,52], the factors surrounding the monitoring stations selected for PM$_{2.5}$ concentration inversion are listed in Table 3. The specific steps include: (1) PM$_{2.5}$ raster data is extracted to point locations, treating these as equivalent to air quality monitoring stations (a total of 520 stations). For each station, meteorological, land use, infrastructural, and socio-economic variables within 100, 200, 300, 500, 750, 1000, 2000, 3000, 4000, and 5000 m buffer zones around the station are calculated. (2) Pearson correlation analysis is conducted between the explanatory variables and PM$_{2.5}$ concentrations, selecting variables that show significant correlations. If the same variable is measured across

Table 3
Variables selected for the LUR model in the study.

Variable type	Variable	Acronym	Note
Land use	Proportion of cropland	Crop	Regarding land use, distribution of POI, and socio-economic development factors, this study calculates values of factors within different buffer zones around the 'site', with the variable expressed as X_distance. For example, Crop_100 indicates the proportion of cropland within the 100-meter buffer zone around the 'site'.
	Proportion of forest	For	
	Proportion of grassland	Gra	
	Proportion of water	Wat	
	Proportion of barren	Bar	
	Proportion of impervious land	Imp	
Distribution of POI	Number of residential sites	Res	
	Number of industrial sites	Ind	
	Number of commercial and financial sites	Com	
	Number of cultural and sports sites	Cul	
	Number of health-care sites	Hea	
	Number of living service sites	Liv	
	Number of road crossings	Cro	
	Number of bus and subway stations	Bus	
Socio-economic development	NTL value	NTL	
	Population density	Pop	
Meteorological feature	SO$_2$ concentration	SO$_2$	Regarding meteorological feature factors, this study calculates values of variables at the 'site' point, without involving buffer zones.
	PM$_{10}$ concentration	PM$_{10}$	
	NO$_2$ concentration	NO$_2$	
	O$_3$ concentration	O$_3$	
	CO concentration	CO	
	Temperature	Tem	
	Precipitation	Pre	

different buffer zones, the one with the strongest correlation at the optimal buffer distance is chosen. (3) A variance inflation factor (VIF) collinearity test is performed on the selected variables, followed by stepwise selection based on a VIF threshold of less than 10. This process results in a refined dataset that includes $PM_{2.5}$ concentrations and a set of explanatory variables for each monitoring station. (4) The dataset is split into training and test sets. The forward stepwise regression analysis is performed on the training set to derive the fitting relationships between the explanatory variables and pollutant concentrations, and the model is validated using the test set. (5) The study area is divided into 360×360 m grids, with each grid center treated as a monitoring station. The explanatory variables for the fitted model are calculated based on the study period, and pollutant concentrations are estimated at each grid point using the fitted model.

3.4. Correlationship analysis

3.4.1. Nonlinear regression model

The nonlinear regression model (NRM) can accurately capture nonlinear correlations and minimize errors in discrete data, while also being able to predict changes and trends in the correlation [54]. NRM can be expressed in various forms, including exponential, power, and logarithmic. In this study, we use the power form, which has been widely used in research on urban climate [58,65]. The formula is as follows:

$$Y_i = \alpha_0 + \sum_{j=1}^{k} \alpha_k X_i^j + \varepsilon_i \qquad (4)$$

Where i represents the urban block; Y_i and X_i represent the dependent variable (LST in summer or $PM_{2.5}$ in winter) and the independent variable (urban morphological metric), respectively; α_0 and α_k represent the intercept and regression coefficients, respectively; ε_i represents the random error term; and k is the order of the polynomial. Eq. (4) describes a linear correlation when $k=1$ and defines a nonlinear correlation when $k>1$. To determine the optimal k for regression, this study progressively increases the order and compares the performance of models with varying orders. The model achieving the best results in cross-validation is selected.

3.4.2. Bootstrapping mediation analysis

Mediation analysis examines the mediating role of certain factors in the effect of the independent variable on the dependent variable (as shown in Fig. 3). This study applies the bootstrap method introduced by Preacher et al. [66] to conduct the mediation analysis. The bootstrap method is a nonparametric resampling procedure that approximates the sampling distribution of the indirect effect without assuming asymptotic normality [55], which has been widely used in fields of urban environments [44,67]. The formulas are as follows:

$$Y = cX + u_1 \qquad (5)$$

$$M = aX + u_2 \qquad (6)$$

$$Y = c'X + bM + u_3 = c'X + abX + u_4 \qquad (7)$$

In Eq. (5)-(7), X, M, Y represent independent variable (urban morphological metric), mediating variable ($PM_{2.5}$ in summer or LST in winter), and dependent variable (LST in summer or $PM_{2.5}$ in winter), respectively; u_1, u_1, u_1, and u_1 represent the random errors; c, c', and ab are the regression coefficients, representing the total effect, direct effect, and indirect effect, respectively. To make the significance test, we performed 5000 bootstrap resamples and calculated 95% bias-corrected confidence intervals (BCIs). The indirect effect is significant if the BCIs do not include zero.

4. Results

4.1. Analysis of urban morphological metrics

Fig. 4 illustrates the spatial performance of urban morphological metrics across urban blocks. It can be observed that the spatial distributions of ABH, SDBH, BD, FAR, and SCD are highly consistent, while their spatial patterns contrast with that of the SVF. Specifically, urban blocks along the West Lake and Qiantang River exhibit higher ABH, BD, FAR, and SCD values. In reality, these areas are popular with residents and attract land developers because of their proximity to an excellent natural environment [68]. Large-volume commercial and public buildings are staggered, while high-density commercial and residential buildings are constructed, bringing high-intensity development to the blocks [69]. As a result, despite being adjacent to water, the average SVF in these areas remains relatively low. The northern part of the West Lake area is also a high-density residential zone, with urban block morphological characteristics similar to those in the waterfront areas. Other urban blocks in the study area are primarily located in the interior, characterized by lower ABH, BD, FAR, and SCD, but higher SVF values. Most of these are residential blocks accommodating similarly sized dwellings [70], leading to high living energy consumption and the formation of localized heat islands [35]. Overall, the urban morphology at the block level in the study area forms a pattern of higher density on the periphery and lower density in the interior, with crowded peripheries and more open interiors. Additionally, the collinearity test results (as shown in Table S1) indicate that there is no collinearity among the variables, suggesting that the selected variables are both concise and effective.

4.2. Analysis of LST and PM2.5 concentration

4.2.1. Results of LST inversion

Fig. 5 illustrates the LST obtained from the inversion in the study area for both summer and winter, along with the average LST further calculated for urban blocks. It can be observed that the average value and range of LST are significantly higher in summer than in winter. Within the study area, forests and water bodies own lower LSTs, while farmland exhibits higher LSTs. The built-up areas generally experience high LSTs, though no distinct hot spots are formed. In urban blocks, the
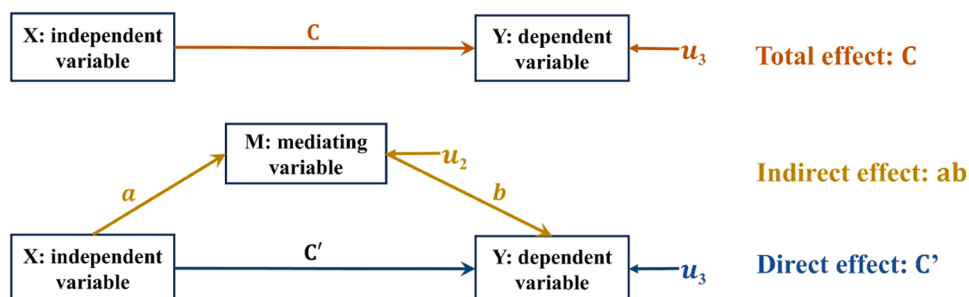
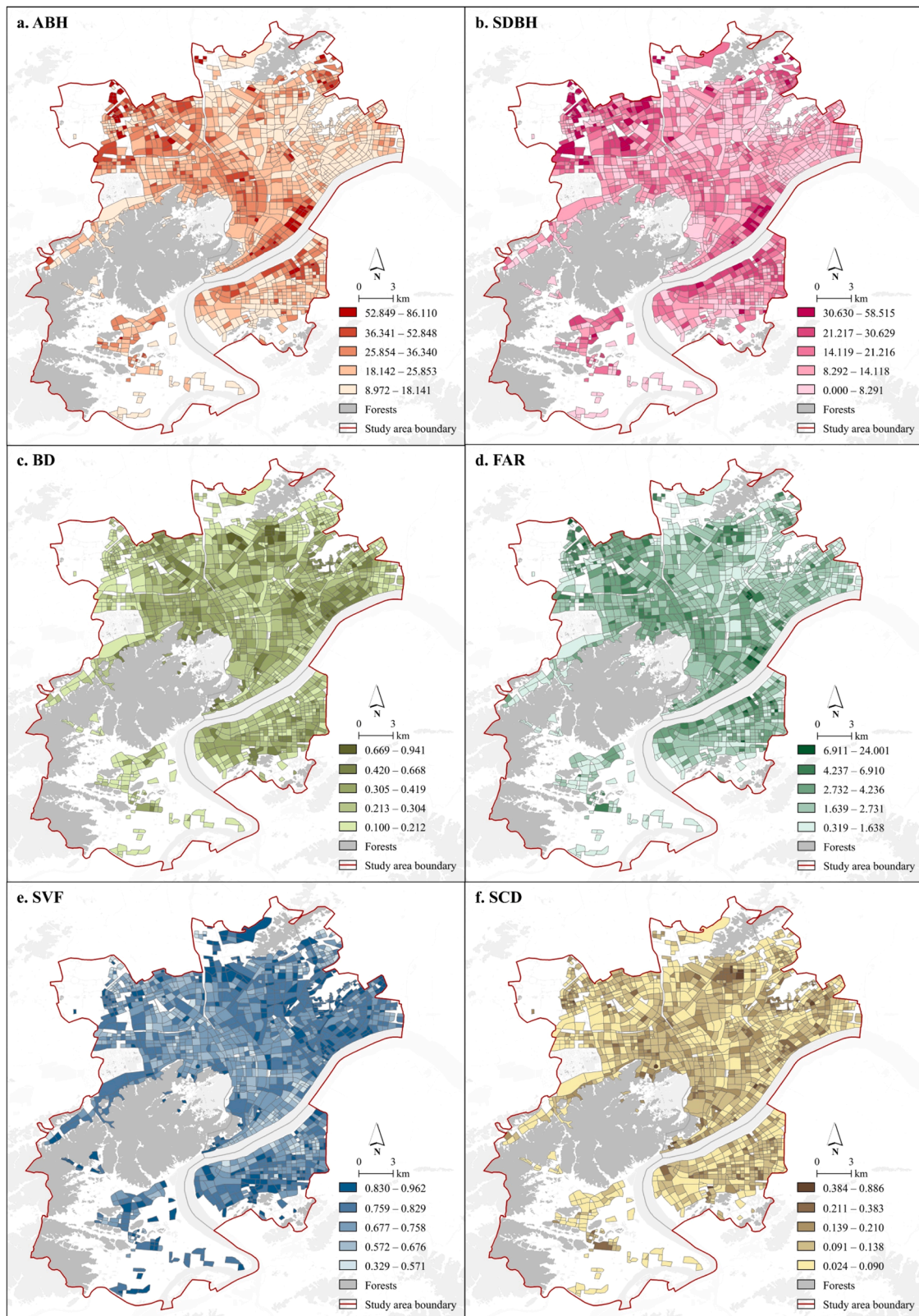**Fig. 3.** Schematic of the mediation analysis model.

Fig. 4. Distribution of urban morphological metrics of blocks.

spatial pattern of the average LST in summer slightly contrasts with that in winter. During the summer, higher average LSTs are observed along the Qiantang River and the Grand Canal. In contrast, during winter, the average LST in these areas is lower, increasing toward the periphery and forming a relatively high-value zone along the West Lake. This reveals that despite their proximity to water bodies, high-intensity block development and dense population dynamics have resulted in significant heat emission and restricted ventilation, contributing to higher LSTs [71].
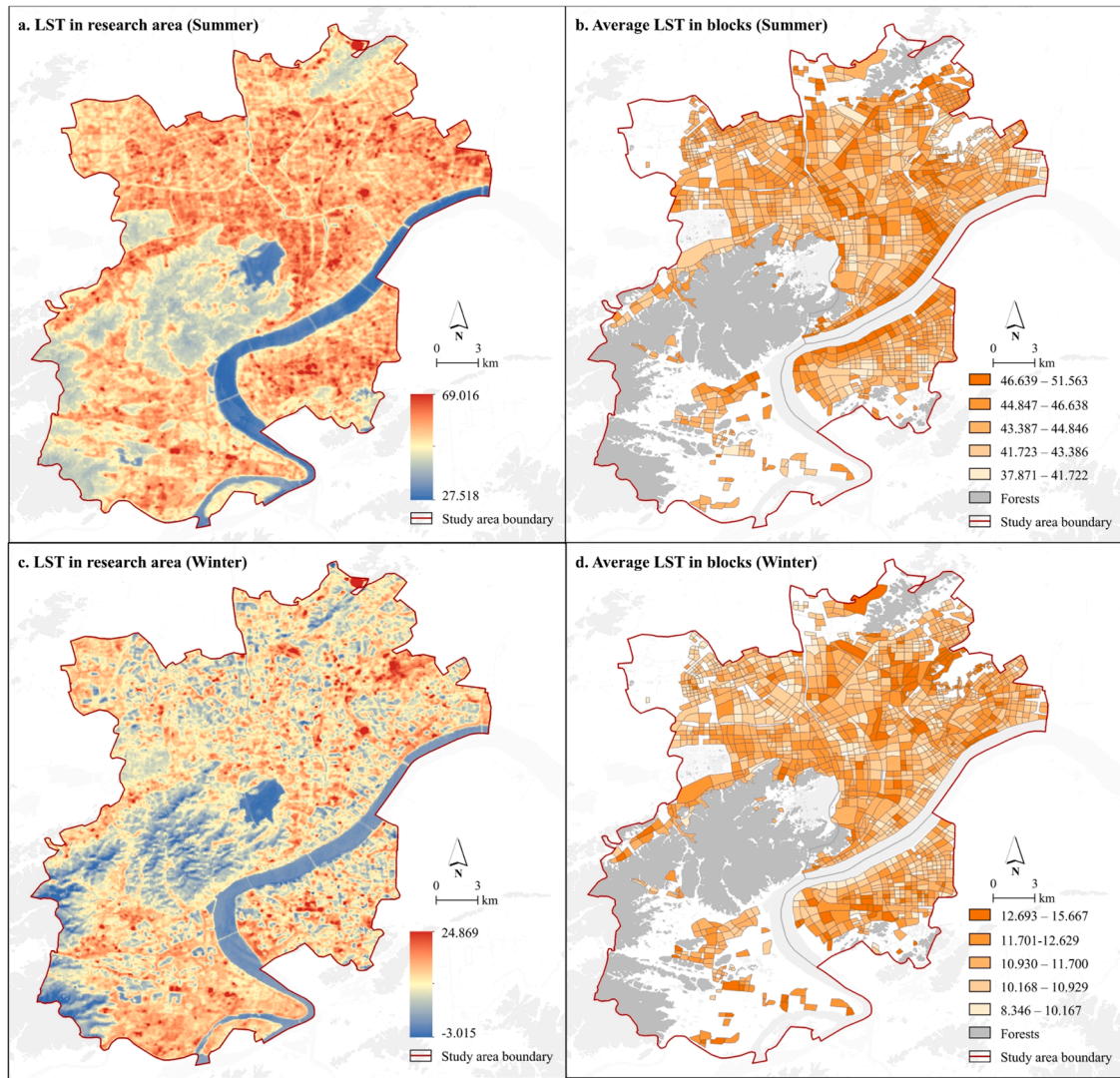
Fig. 5. LST in the research area and average LST in blocks in summer and winter.

4.2.2. Results of PM₂.₅ downscaling

Table 4 presents the regression variables and coefficients of the LUR models for PM₂.₅ in the study area during summer and winter, derived from the training dataset. Fig. 6 illustrates the performance of the fitted models on the test dataset. A total of 11 and 7 variables were included in the summer and winter LUR models, respectively, with the models

Table 4
Results of LUR model for PM₂.₅ in summer and winter.

| Summer (R^2 = 0.747)			Winter (R^2 = 0.858)		
Variable	Coefficient	P_value	Variable	Coefficient	P_value
Crop_5000	-2.552e-8	0.000***	Crop_5000	-3.993e-9	0.000***
For_5000	-1.903e-8	0.000***	For_5000	-9.639e-8	0.000***
Gra_5000	1.000e-4	0.000***	Gra_5000	1.000e-4	0.004**
Wat_4000	5.061e-8	0.000***	Pop_500	1.220e-2	0.000***
Bar_5000	-7.548e-8	0.002**	NTL_2000	4.070e-2	0.000***
Ind_5000	1.820e-2	0.000***	Pre	6.560e-2	0.000***
Cul_4000	1.300e-3	0.000***	Tem	1.415e0	0.000***
Cro_5000	-2.100e-3	0.000***	Const	3.195e1	0.000***
Bus_2000	3.400e-3	0.000***	-	-	-
Pop_200	2.500e-3	0.010*	-	-	-
Pre	7.370e-2	0.000***	-	-	-
Const	3.949e1	0.000***	-	-	-

Note: as for the significance test, * represents P_value < 0.1; ** represents P_value < 0.01; *** represents P_value < 0.001.

achieving explanatory powers of 0.810 and 0.843. These results indicate that the model fitting accuracy is reliable for PM₂.₅ prediction. Further details on the construction of the LUR models can be found in Text S1 and Tables S1-S4.

Furthermore, the PM₂.₅ concentrations at a 360 m resolution for both summer and winter were calculated for the study area based on the obtained LUR models, and the average PM₂.₅ concentrations for each urban block were computed (as shown in Fig. 7). It can be observed that both the average value and range of PM₂.₅ concentrations are higher in winter than in summer. A distinct PM₂.₅ pollution island phenomenon is evident in the study area. Notably, ecological spaces such as the West Lake Scenic Area and Xixi Wetland are characterized by low PM₂.₅ concentrations, while the built-up areas exhibit higher values. This can be directly attributed to the higher concentration of particulate matter emissions and relatively poor ventilation conditions in the urban center [30]. Additionally, the locations of high-value zones exhibit seasonal variability, which may be related to the prevailing wind direction in Hangzhou [58]. In summer, the eastern shore of West Lake and the western part of Binjiang are identified as high PM₂.₅ concentration areas, with urban blocks in these regions also experiencing higher average PM₂.₅. In winter, the eastern part of Binjiang and the central areas of the West Lake, Gongshu, and Shangcheng emerge as high-value zones. The high-value area along the northern bank of the Qiantang River exhibits a linear, parallel pattern, suggesting a potential
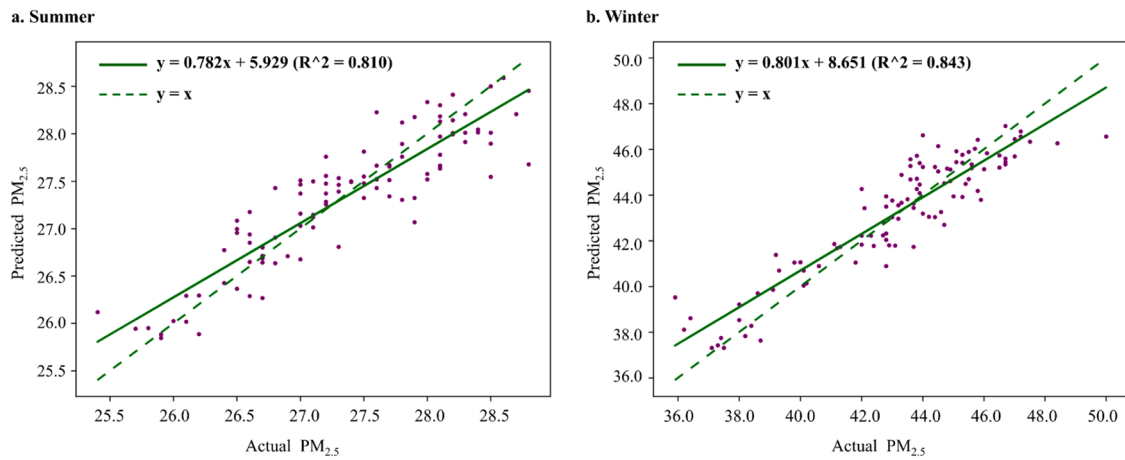
Fig. 6. Scatter plots showing actual and predicted PM$_{2.5}$ in the test dataset using the LUR model.
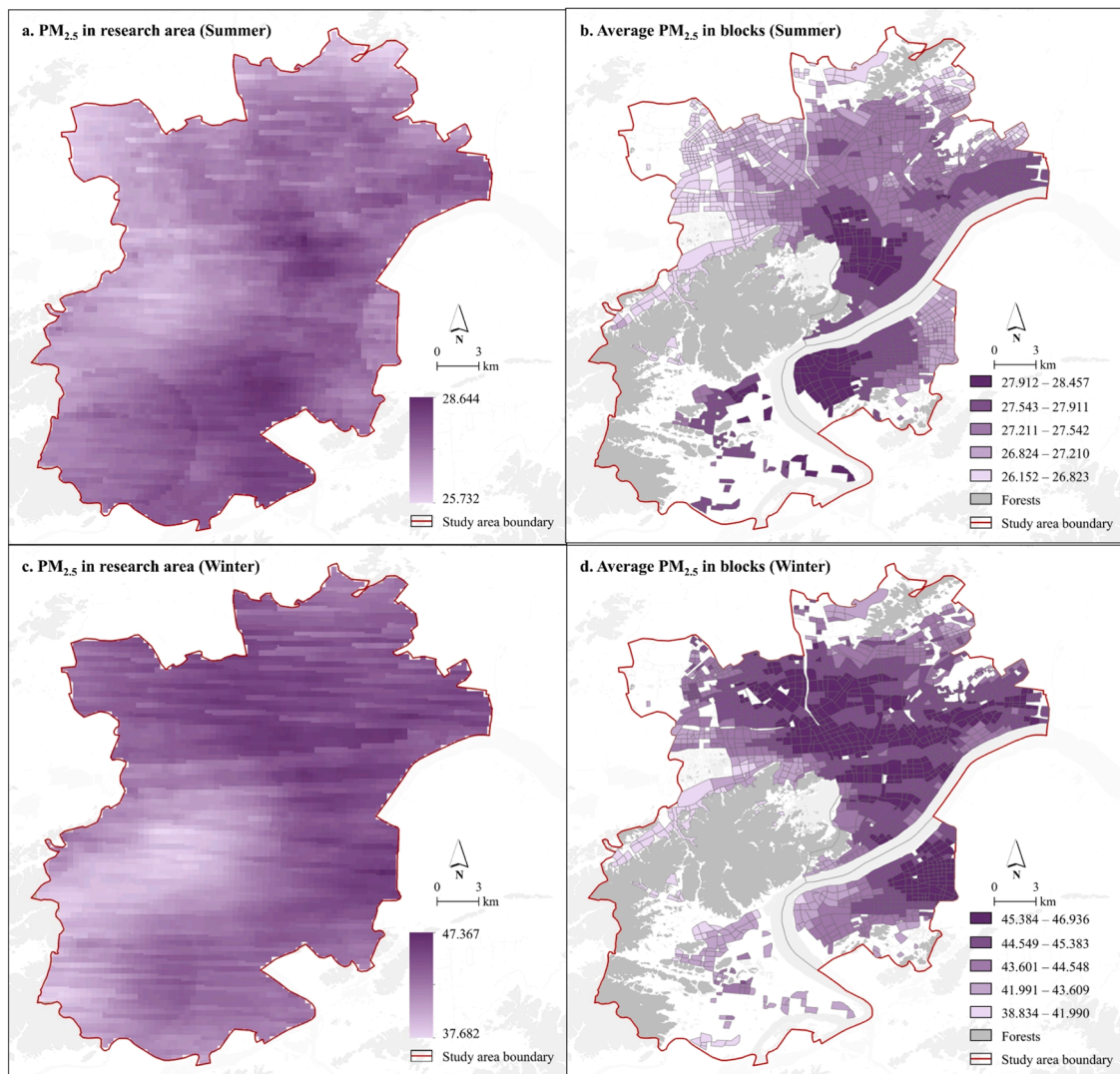
Fig. 7. PM$_{2.5}$ in the research area and average LST in blocks in summer and winter.

correlation with the layout of the urban primary roads [19].

4.2.3. Combined performance of LST and PM$_{2.5}$ in blocks

Furthermore, this study classified the overall performance of both

LST and PM$_{2.5}$ in urban blocks using the quadrant method, with the average values of LST and PM2.$_5$ in each block as the origin (as shown in Fig. 8). It was observed that the classification results show a significant consistency between summer and winter. To the north of the Qiantang
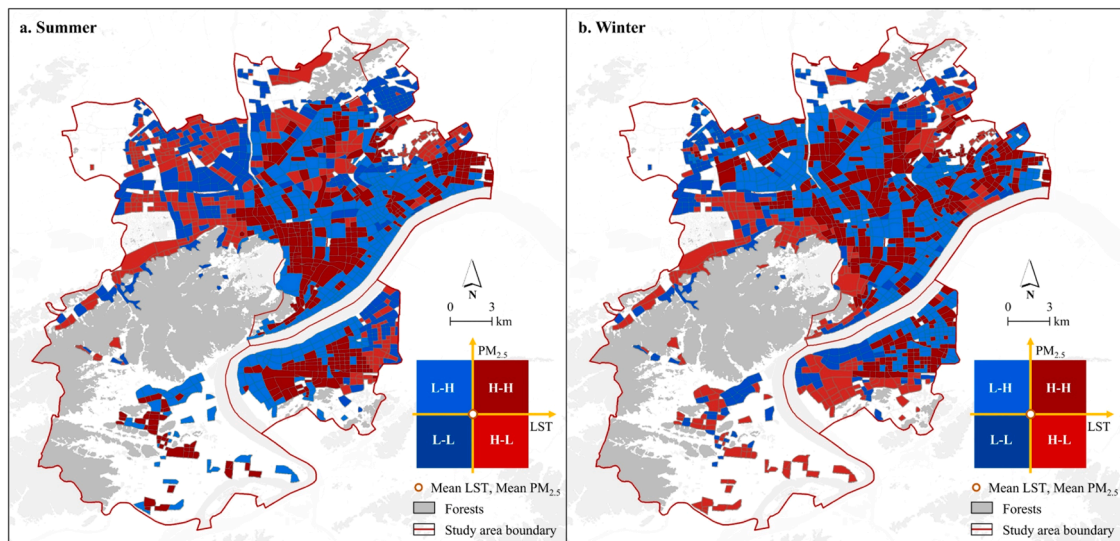
Fig. 8. Combined performance of LST-PM$_{2.5}$ of urban blocks in summer and winter.

River, the high LST-low PM$_{2.5}$ and low LST-high PM$_{2.5}$ groups are distributed in an intersecting pattern in the central urban area, while a high LST-high PM$_{2.5}$ group is found around the West Lake Scenic Area. On the southern bank of the Qiantang River in Binjiang, low LST-low PM$_{2.5}$ blocks are located along the river, while high LST-high PM$_{2.5}$ blocks characterize the southern part of Binjiang. This phenomenon suggests that areas around urban scenic spots, due to intense development, may experience poorer environmental conditions. However, large-scale mountainous or water areas may mitigate this risk [71].

4.3. Effects of urban morphology on LST (summer) and PM$_{2.5}$ (winter)

4.3.1. Nonlinear effects

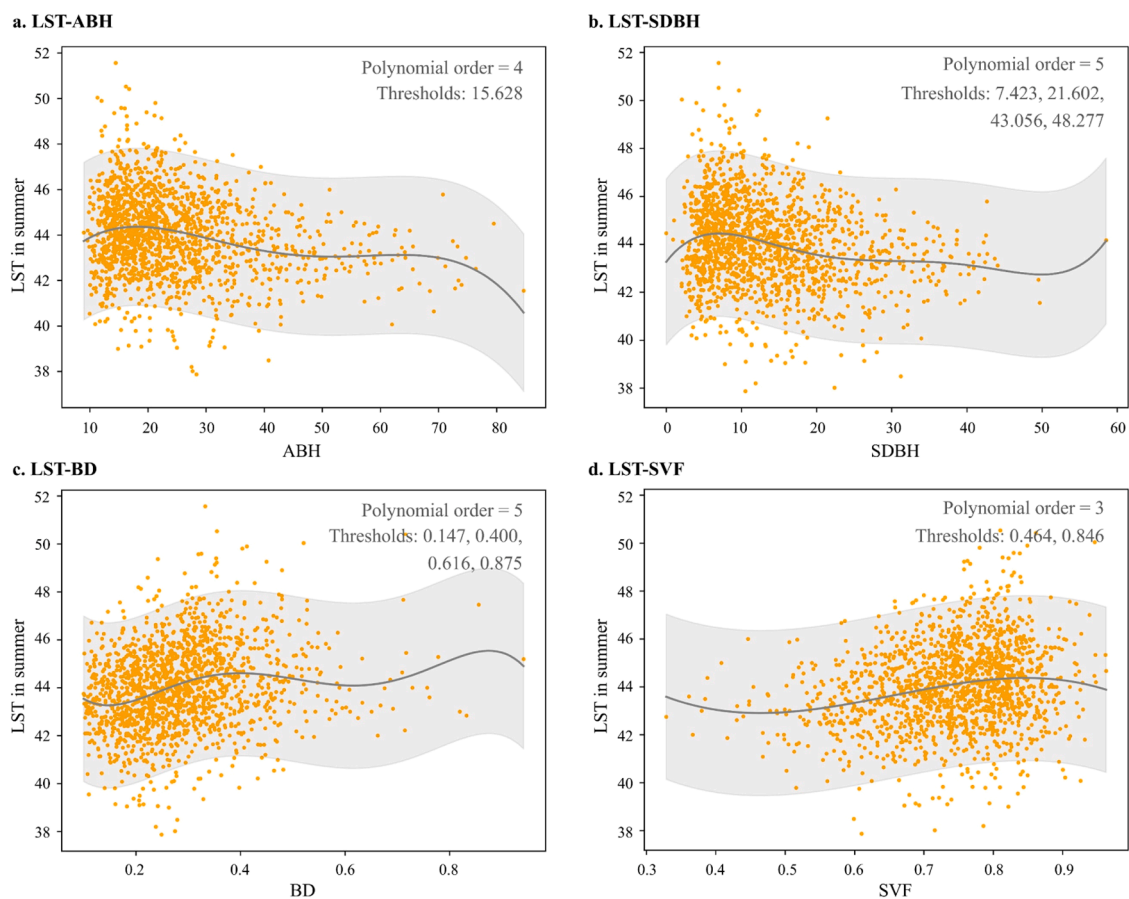The nonlinear effects of urban morphology on summer LST and

Fig. 9. Nonlinear fitting graphs of urban morphology and LST in summer.
Note: the regressions for both LST-FAR and LST-SCD failed, as the regression coefficients did not pass the significance test (as described in Table S6).

winter PM$_{2.5}$ are identified by NRM. Determination of the optimal orders and fitting results of NRMs are described in Text S2, Table S6, and Fig. S1-S2.

Fig. 9 presents the nonlinear effects of urban morphology on LST in summer. ABH exhibits a fourth-order nonlinear correlation with LST in summer. A positive correlation is observed when ABH < 15.628, while a negative correlation occurs when ABH > 15.628. Most urban blocks in the study area have ABH values concentrated between 0 and 30, with slightly more blocks having ABH values greater than 15. SDBH and BD display complex fifth-order nonlinear correlations with LST in summer, each with four thresholds for positive and negative correlation changes. SDBH is positively correlated with LST until it reaches the first threshold, after which the correlation alternates between negative and positive. In contrast, BD exhibits an inverse pattern: first showing a negative and later a positive correlation. Most SDBH and BD values in the urban blocks are concentrated within their first two value intervals, with more blocks falling within the second range (21.602–43.056 for SDBH and 0.400–0.616 for BD). Chen et al. [36] found that SDBH is negatively correlated with LST, as larger differences in building height can enhance shading effects from taller buildings. We hypothesize that when building height variation is minimal, it fails to provide adequate shading and may even hinder the formation of air corridors. SVF has a three-stage nonlinear effect on LST in summer. The relationship initially performs negatively, then positively, and finally negatively again. Nearly all urban blocks have SVF values between 0.464 and 0.846.

Fig. 10 presents the nonlinear effects of urban morphology on PM$_{2.5}$ in winter. Both ABH and BD exhibit a third-order nonlinear correlation with PM$_{2.5}$ in winter. This relationship is characterized by an initial positive correlation, followed by a negative correlation, and then another positive correlation. Most urban blocks in the study area have ABH and BD values below their first thresholds (31.387 and 0.358, respectively). SDBH shows a complex fourth-order nonlinear correlation with PM$_{2.5}$ concentrations in winter, with a positive correlation when SDBH < 11.133, and a negative correlation otherwise. The majority of urban blocks in the study area have SDBH values concentrated between 0 and 20, with more blocks having values less than 11.133. FAR, SVF, and SCD all exhibit nonlinear relationships with PM$_{2.5}$ in winter,

initially positive, followed by negative. The thresholds for these relationships are approximately 5.457, 0.600, and 0.313, respectively. The negative shift may relate to the association between high FAR and high-rise, low-density urban morphology [72], the threshold for SVF in regulating airflow, and the link between SCD and the narrow-channel effect on air circulation. Within the study area, nearly all urban blocks do not reach the threshold for FAR and SCD, while slightly more blocks have SVF values above the threshold than below it.

4.3.2. Total, direct, and indirect effects

Table 5 presents the bootstrapping mediation analysis results, showing that all effects are statistically significant. Regarding the total effect, ABH, SDBH, and FAR are negatively correlated with LST in summer, while BD, SVF, and SCD are positively correlated. Except for SVF, all urban morphology metrics exhibit a positive correlation with PM$_{2.5}$ in winter. Notably, nonlinear correlations between urban morphology and LST/PM$_{2.5}$ were observed using NRM in the preceding analysis. However, urban morphology values in most urban blocks are concentrated within a specific range, not reaching the threshold that would alter the effect direction. As a result, the total effect of a specific metric on LST/PM$_{2.5}$ is in the same direction as the effects of its majority values.

Furthermore, the impact of urban morphology on LST in summer is primarily realized through direct effects. Specifically, PM$_{2.5}$ in summer effectively transmits the effects of ABH and FAR in lowering LST, and BD, SVF, and SCD in raising LST. However, the mediating effect is limited: the largest mediation effect is 2.146% for the effect of FAR on LST, while the other effects do not exceed 1%. Meanwhile, PM$_{2.5}$ in summer suppresses the effect of SDBH on lowering LST, but this suppression only affects 0.304% of the originally negative effect. In contrast, the impact of urban morphology on PM$_{2.5}$ in winter is significantly mediated by LST in winter. Specifically, LST fully mediates the positive effects of both ABH and SDBH on PM$_{2.5}$, while mediating 9.032% of the positive effect of FAR on PM$_{2.5}$ and 17.278% of the negative effect of SVF on PM$_{2.5}$. The positive effects of BD and SVF on PM$_{2.5}$ are suppressed by LST, with the suppression reducing the total effect by absolute values of 10.187% and 11.741%, respectively.
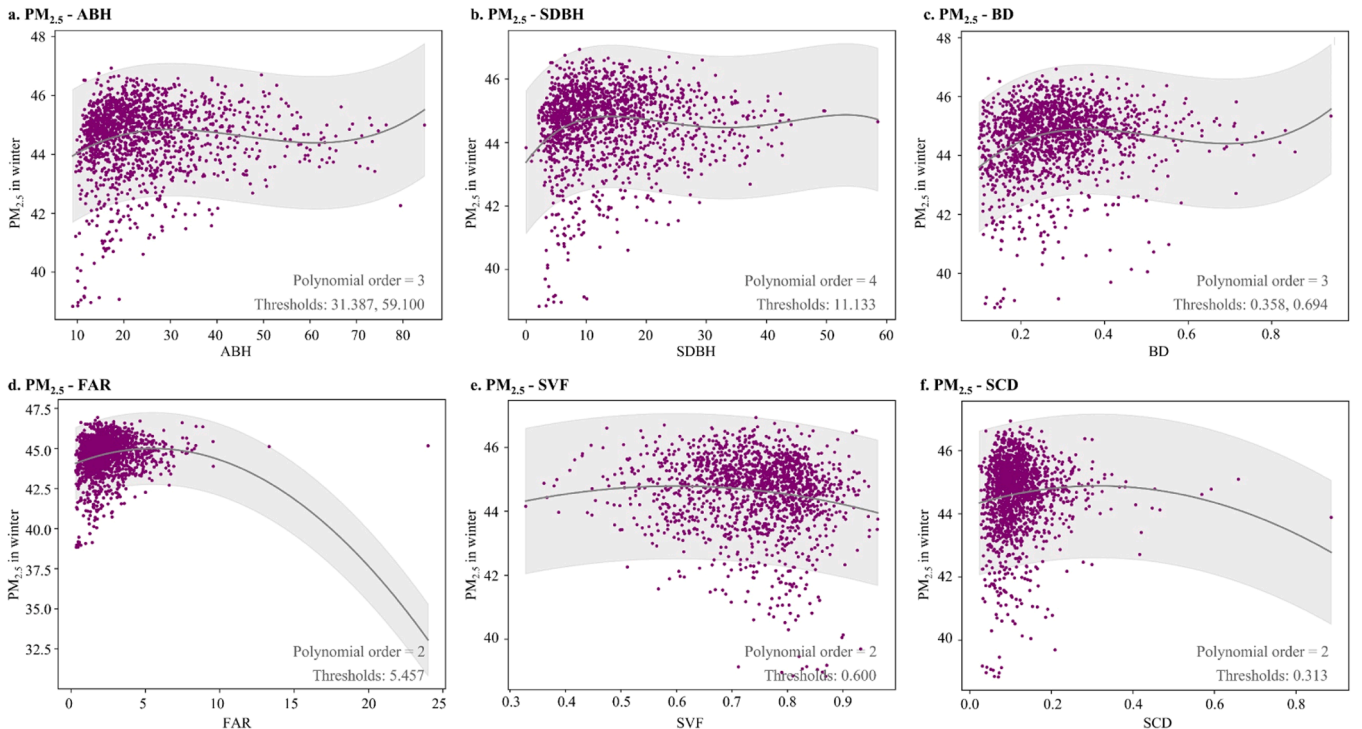

Fig. 10. Nonlinear fitting graphs of urban morphology and PM$_{2.5}$ in winter.

Table 5
Results of the bootstrapping mediation analysis.

Dependent variable	Mediating variable	Independent variable	Indirect effect		Direct effect		Total effect		Proportion mediated
			ab	95% BCI	*c'*	95% BCI	*c*	95% BCI	
LST in summer	PM$_{2.5}$ in summer	ABH	-0.000	(-0.001, -0.000)	-0.031	(-0.038, -0.024)	-0.031	(-0.038, -0.024)	0.323%
		SDBH	+0.000	(+0.000, 0.002)	-0.046	(-0.056, -0.036)	-0.046	(-0.056, -0.036)	-0.304%
		BD	0.021	(0.016, 0.026)	2.958	(2.261, 3.655)	2.979	(2.285, 3.672)	0.715%
		FAR	-0.001	(-0.002, -0.000)	-0.046	(-0.078, -0.013)	-0.047	(-0.082, -0.012)	2.146%
		SVF	0.025	(0.023, 0.029)	3.783	(2.892, 4.674)	3.808	(2.917, 4.698)	0.649%
		SCD	0.042	(0.031, 0.054)	4.825	(3.480, 6.170)	4.867	(3.524, 6.210)	0.863%
PM$_{2.5}$ in winter	LST in winter	ABH	0.003	(0.001, 0.005)	0.004	(-0.001, 0.010)	0.007	(0.002, 0.012)	100.000%
		SDBH	0.005	(0.002, 0.008)	0.004	(-0.004, 0.011)	0.009	(0.002, 0.015)	100.000%
		BD	-0.157	(-0.255, -0.084)	1.539	(1.073, 2.006)	1.383	(0.918, 1.848)	-10.187%
		FAR	0.011	(0.002, 0.021)	0.112	(0.072, 0.152)	0.123	(0.084, 0.162)	9.032%
		SVF	-0.250	(-0.478, -0.024)	-1.194	(-1.840, -0.549)	-1.444	(-2.044, -0.844)	17.278%
		SCD	-0.159	(-0.301, -0.059)	1.515	(0.613, 2.418)	1.356	(0.453, 2.259)	-10.507%

Note: (1) when the indirect effect is in the same direction as the total effect, proportion mediated $= ab/c$; when the indirect effect is in the opposite direction as the total effect, proportion mediated $= ab/(c - ab)$; (2) proportion mediated equals 100.000% when the direct effect is insignificant.

Considering that PM$_{2.5}$ is lower in summer and LST is lower in winter, it suggests that low LST in winter significantly impacts the atmospheric environment, whereas low PM$_{2.5}$ in summer has a limited effect.

5. Discussion

5.1. Applying LUR model to downscale PM$_{2.5}$

Downscaling refers to the process of converting large-scale, low-resolution data into finer-scale, high-resolution data [73]. Li et al. classified downscaling methods into three categories [74]. One effective approach is to establish a relationship between the explained elements and relevant explanatory variables, and then downscale the original data based on the established equations [75]. This method has already been applied in the downscaling of LST [59,76]. This study adopts the same method for downscaling PM$_{2.5}$ but with its unique characteristics. On the one hand, LST regression uses temperature and other features within the grid as variables, assuming that the correlations of these variables within grids at different scales remain constant [77]. In contrast, the LUR model applied in this study uses buffer zone data around monitoring points as independent variables, eliminating the need for the assumption required in the LST downscaling. Additionally, the selection of buffer zones at varying distances considers the pollutants' mobility and the variables' spatial effects. On the other hand, LUR can directly infer pollutant concentrations based on air monitoring station data [78]. In this study, we treat the central points of grids in the open-source raster data as air monitoring stations and perform the inversion as part of the downscaling process, offering the advantages of lower cost and greater scalability. It is important to note that the method used in this study has a limitation. The 1 km resolution PM$_{2.5}$ data employed were already derived through inversion based on various socio-economic conditions, meaning further establishing relationships may introduce redundancy and complexity. Nonetheless, we believe this method still provides a feasible approach for obtaining high-resolution pollutant data in areas lacking air quality monitoring stations.

5.2. Understanding of combined effects

The study reveals the nonlinear effects of urban morphology on LST/PM$_{2.5}$ using NRM. High LST/PM$_{2.5}$ concentrations result from the emission, circulation, and accumulation of massive heat/particulate matter [79,80]. Urban morphology directly intervenes in processes of circulation and accumulation by affecting local microclimates [25,26], especially radiation and airflow. Moreover, urban morphology can reflect and reshape human behavior and socio-economic conditions [19, 28], affecting heat and particulate matter emissions. These effects exert simultaneously and balance mutually, leading to different effects as urban morphology enters different value ranges. Therefore, based on the identified nonlinear correlations and relevant studies, we integrate the impact of urban morphology on factors such as local climate and socio-economic status to infer the potential underlying mechanisms. Take ABH and BD for example, (1) ABH reflects population density, social dynamics, and buildings' ability to block radiation and airflow. Specifically, higher ABH corresponds to a higher population density when the overall level of ABH is low. This leads to more heat and pollutant sources, resulting in elevated LST and PM$_{2.5}$ [10]. As ABH continues to increase, the need for sunlight results in a sparser building layout, thereby enhancing ventilation capacity [37]. Consequently, this study observed a nonlinear relationship between ABH and LST/PM$_{2.5}$, characterized by an initial positive correlation followed by a negative correlation. This finding aligns with the findings of Zhang et al. [81] in Shanghai. Nevertheless, further increases in ABH gradually form deep canyons within urban blocks, causing PM$_{2.5}$ to accumulate and rise again [82]. (2) BD influences the light intensity within urban blocks, while also reflecting residential patterns. Most studies have found that higher BD leads to higher PM$_{2.5}$ [33,34] and elevated LST [35,36]. However, this study reveals a negative correlation between BD and PM$_{2.5}$ within the range of 0.36 to 0.69, while up to four positive and negative transitions exist in the relationship between BD and LST. Regarding this, we propose that a moderate increase in BD may not lead to a corresponding rise in energy consumption, as the reduction due to higher resource utilization efficiency from technological progress could

offset it. Besides, fewer building patches at the same BD may also help mitigate the negative impacts of BD.

This study examined the effect of urban morphology on $PM_{2.5}$ affecting LST in summer, as well as the effect of urban morphology on LST affecting $PM_{2.5}$ in winter. This interaction is primarily mediated through the complex relationship between LST and $PM_{2.5}$. (1) The influence of urban morphology on $PM_{2.5}$ would affect LST in summer, but the effects are relatively weak (less than 2.2%). Previous studies suggest that $PM_{2.5}$ can absorb shortwave solar radiation to create a cooling effect [31], while also absorbing longwave radiation from the ground to promote the greenhouse effect [83]. We propose that these opposing effects of $PM_{2.5}$ may balance each other in Hangzhou during summer, limiting its mediating role. Additionally, lower $PM_{2.5}$ concentrations in most urban blocks may also contribute to this phenomenon [84]. High $PM_{2.5}$ concentrations are mostly found around West Lake and the Qiantang River, where their impact on LST is somewhat mitigated by water bodies [85]. (2) LST significantly mediates the effects of urban morphology on $PM_{2.5}$ in winter, where LST and $PM_{2.5}$ are negatively correlated. The effects of urban morphology on winter $PM_{2.5}$ through LST all exceed 9.0%, stronger than the impact of $PM_{2.5}$ on summer LST. Notably, LST fully mediates the relationship between building height and $PM_{2.5}$, with higher ABH generally linked to lower LST and higher $PM_{2.5}$ in most blocks. Specifically, lower LST hinders atmospheric convection, potentially causing atmospheric inversion [86]. It also reduces turbulence and lowers the mixing layer height, increasing atmospheric stability [32]. As a result, $PM_{2.5}$ tends to accumulate in source blocks and near the ground due to the lack of airflow for dispersion. The negative correlation aligns with some studies [44,87,88] but contradicts findings by Ngarambe et al. [32] and Liang et al. [43]. Variations in $PM_{2.5}$ concentrations [84] and particle size [89] may explain these opposing results. Therefore, further multi-scenario simulations of thermal and atmospheric environments are needed.

5.3. Implications for urban block planning

Based on the research findings, it can be seen that block planning does not favor extreme values for urban morphological metrics. Indeed, the key lies in the control of degree and the combination of morphological metrics. Based on the overall conditions of the study area and the context of urban planning and redevelopment, we propose several potential planning strategies for urban blocks: (1) opt for a mid- to high-rise, low-density building mode. When ABH is between 20-60 m and BD ranges from 0.2 to 0.4, a high-rise, low-density development mode promotes the creation of open channels, facilitating atmospheric circulation. This development approach is also advocated in the studies of Yuan et al. [90] and Liu et al. [91]. (2) The degree of spatial openness and building height variation should either be high or low, as intermediate values may not be optimal. When SVF is between 0.46 and 0.85, the block provides space for particulate matter, but the wind generated is not sufficient to offset the heat from solar radiation. The benefits of high openness have also been validated in related studies [92]. Similarly, when SDBH exceeds 4, the cooling and pollution-reducing effects in the block become significant. (3) FAR and SCD should be reduced to reduce $PM_{2.5}$, which is consistent with existing planning strategies. Additionally, attention should be given to analyzing and controlling the building's thermal environment, as it can significantly influence particulate matter concentrations during the winter. Specifically, this can be done through computer-based numerical simulations [86].

Additionally, urban waterfront areas have garnered widespread attention because of their abundant blue and green spaces [93]. Some studies suggest that water bodies are inherently cleaner as substitutes for built-up land [78] and can reduce heat and $PM_{2.5}$ by increasing wind speed and humidity [94,95]. However, our study observed the opposite phenomenon: urban blocks around West Lake and along the Grand Canal simultaneously experience high LST and $PM_{2.5}$ concentrations. Moreover, we found that these areas also exhibit high ABH, BD, FAR,

and SCD. This may be attributed to the increased land value driven by the attractive waterfront views, which encourage more intensive urban development [68]. Therefore, this study suggests that high-intensity development around quality urban water bodies may hinder local airflow exchange, resulting in more severe heat and air pollution compared to the core urban area. This finding aligns with the results of Wang et al. [71]. To mitigate this issue, we propose that waterfront blocks focus more on controlling building height and density. Specifically, we suggest exploring mid- to high-rise, low-density designs that do not compromise the visual integrity of urban water bodies, while actively reserving wind corridors to introduce clean air into the urban area [96].

Furthermore, effective guarantee institutions should be established to support the implementation of planning strategies [97]. Potential government measures include: (1) Developing location-specific optimization standards for urban block morphology through expanded scientific research; (2) Promoting specialized planning initiatives to improve thermal and atmospheric environments, such as updating older blocks and implementing pilot projects for representative blocks; (3) Providing technical support and financial incentives, such as 3D simulation modeling of building clusters and rewards for achieving morphological standards. Additionally, strategies to encourage public participation include: (1) Raising public awareness of the relationship between urban morphology and thermal/atmospheric environments; (2) Establishing reward mechanisms to motivate residents to actively monitor changes in block morphology.

5.4. Contributions and limitations

The marginal contributions of this study to scientific research and practical application are as follows: (1) Proposing the feasibility of using the LUR model to downscale large-scale, low-resolution $PM_{2.5}$ data, further advancing research on the atmospheric environment across fine-scale urban blocks within the city. Analyzing haze pollution across urban blocks aligns with urban planning and environmental governance needs. However, station monitoring, mobile monitoring, and meteorological simulations are costly within the entire city, limiting their practical use. By converting open-source raster data to equivalent point data, the LUR model can downscale and generate high-resolution $PM_{2.5}$ data. Additionally, the relationship between point values and surrounding buffer variables is more transferable than the grid-based relationships used in traditional LST downscaling. (2) Revealing nonlinear and potential mediating effects of urban morphology on the LST in summer and $PM_{2.5}$ in winter. NRM seeks the optimal nonlinear relationship by gradually increasing the order of fitting. This allows for a deeper understanding of the complex nonlinear correlations between urban morphology and LST/$PM_{2.5}$, beyond the linear or simple quadratic correlations found in previous studies. Bootstrapping mediation analysis explored the potential mediating mechanisms of $PM_{2.5}$ between urban morphology and LST, and vice versa. This provides initial insights into the possibilities of coordinated control of heatwaves and haze pollution. (3) Research findings on the combined effects of urban morphology on LST and $PM_{2.5}$ provide reasonable references for optimizing urban block morphologies to improve thermal and atmospheric environments. The identified key morphological metrics and their threshold values can serve as standards for morphological optimization. Waterfront areas with significant conflicts between block development and environmental protection can be prioritized in urban planning.

The study acknowledges several limitations. (1) This study has made efforts to refine the research object at the spatial scale; however, at the temporal scale, it still relied on daily average data. Both LST and $PM_{2.5}$ exhibit significant variations throughout the day and even on an hourly basis. Future studies could explore data across multiple periods to better understand the heat and pollution dynamics within urban blocks across the city. (2) This study inferred the potential mechanisms by which

urban morphology affects LST and PM$_{2.5}$ through statistical correlation analysis. However, the complex three-dimensional interactions between LST, PM$_{2.5}$, and urban morphology, along with the influence of socio-economic and meteorological factors, complicate the understanding of these mechanisms. Future studies could combine 3D simulations of typical urban blocks with multivariate statistical regression models for a deeper analysis of these underlying mechanisms. (3) This study focused solely on Hangzhou as the research area. Climate conditions and urban construction practices vary significantly across different regions. Future research could analyze more cities to explore inter-city differences.

6. Conclusions

The resolution of pollutant concentration data has ever limited the analysis of the thermal and atmospheric environments across all fine-scale urban blocks within the city. This study applied the LUR model to downscale open-source PM$_{2.5}$ data while also integrating remote sensing-derived LST to identify the LST and PM$_{2.5}$ concentrations across all urban blocks in the core area of Hangzhou. An interesting finding is that waterfront blocks are more likely to experience both high LST and elevated PM$_{2.5}$ concentrations due to high-intensity development.

Identifying the combined effects of urban morphology on LST and PM$_{2.5}$ can provide valuable insights for optimizing urban block planning. In this study, we applied NRM to compute the nonlinear effects of urban morphology on summer LST and winter PM$_{2.5}$, while bootstrapping mediation analysis was used to identify the indirect effects of urban morphology on LST through PM$_{2.5}$ in summer and on PM$_{2.5}$ through LST in winter. The results revealed nonlinear correlations between ABH, SDBH, BD, SVF, and both summer LST and winter PM$_{2.5}$, while FAR and SCD exhibited nonlinear effects only on PM$_{2.5}$. Most urban blocks had morphological values that did not exceed thresholds, which explains the unidirectional total effects of urban morphology on LST/PM$_{2.5}$. Additionally, urban morphology significantly influenced PM$_{2.5}$ concentrations in the winter through LST, while the effect of urban morphology on LST through PM$_{2.5}$ was minimal in summer. LST fully mediated the effects of ABH and SDBH on PM$_{2.5}$.

Based on the research findings, we propose block planning approaches that favor the selection of mid- to high-rise, low-density building modes (with ABH ranging from 20-60 m and BD between 0.2-0.4), increasing the spatial openness within blocks (with SVF greater than 0.85), and enhancing the building height difference (with SDBH > 4). This study aims to uncover potential approaches for analyzing the thermal and atmospheric environments of fine-scale urban blocks and provides possible strategies through urban morphological design.

CRediT authorship contribution statement

Xin Chen: Writing – review & editing, Writing – original draft, Visualization, Software, Methodology, Formal analysis, Data curation, Conceptualization. **Fang Wei:** Writing – review & editing, Supervision.

Declaration of competing interest

The authors declare that they have no known competing financial interests or personal relationships that could have appeared to influence the work reported in this paper.

Supplementary materials

Supplementary material associated with this article can be found, in the online version, at doi:10.1016/j.buildenv.2025.112979.

Data availability

Data will be made available on request.

Reference

[1] C. Hu, M. Zhang, G. Huang, Z. Li, Y. Sun, J. Zhao, Tracking the impact of the land cover change on the spatial-temporal distribution of the thermal comfort: insights from the Qinhuai River Basin, China, sustain, Cities Soc. 116 (2024) 105916, https://doi.org/10.1016/j.scs.2024.105916.

[2] M. Zhang, E. Chen, C. Zhang, C. Liu, J. Li, Multi-scenario simulation of land use change and ecosystem service value based on the Markov–FLUS model in Ezhou City, China, Sustainability 16 (2024) 6237, https://doi.org/10.3390/su16146237.

[3] M. Zhang, İ. Yiğit, F. Adigüzel, C. Hu, E. Chen, A.E. Siyavuş, N. Elmastaş, M. Ustuner, A.Y. Kaya, Impact of urban surfaces on microclimatic conditions and thermal comfort in Burdur, Türkiye, Atmosphere (Basel) 15 (2024) 1375, https://doi.org/10.3390/atmos15111375.

[4] N. Okamoto, Spatial and institutional urbanisation in China, Asia-Pac. J. Reg. Sci. 3 (2019) 863–886, https://doi.org/10.1007/s41685-019-00113-y.

[5] A. Wang, M. Zhang, E. Chen, C. Zhang, Y. Han, Impact of seasonal global land surface temperature (LST) change on gross primary production (GPP) in the early 21st century, Sustain. Cities Soc. 110 (2024) 105572, https://doi.org/10.1016/j.scs.2024.105572.

[6] L. Inostroza, H. Taubenböck, Searching for the DNA of urbanisation. A material perspective, Cities 151 (2024) 105079, https://doi.org/10.1016/j.cities.2024.105079.

[7] B.M. Saunders, J.D. Smith, T.E.L. Smith, D.C. Green, B. Barratt, Spatial variability of fine particulate matter pollution (PM2.5) on the London Underground network, Urban Clim 30 (2019) 100535, https://doi.org/10.1016/j.uclim.2019.100535.

[8] A. Wang, M. Zhang, B. Ren, Y. Zhang, A.-A. Kafy, J. Li, Ventilation analysis of urban functional zoning based on circuit model in Guangzhou in winter, China, Urban Clim. 47 (2023) 101385, https://doi.org/10.1016/j.uclim.2022.101385.

[9] J. Song, W. Chen, J. Zhang, K. Huang, B. Hou, Effects of building density on land surface temperature in China: spatial patterns and determinants, Landsc. Urban Plan. 198 (2020) 103794, https://doi.org/10.1016/j.landurbplan.2020.103794.

[10] W. Ding, S. Liu, Impact assessment of air pollutants and greenhouse gases on urban heat wave events in the Beijing–Tianjin–Hebei region, Environ. Geochem. Health 45 (2023) 7693–7709, https://doi.org/10.1007/s10653-023-01677-7.

[11] Y. Li, Y. Zhang, Q. Wu, R. Xue, X. Wang, M. Si, Y. Zhang, Greening the concrete jungle: unveiling the co-mitigation of greenspace configuration on PM2.5 and land surface temperature with explanatory machine learning, Urban For. Urban Green 88 (2023) 128086, https://doi.org/10.1016/j.ufug.2023.128086.

[12] N. Watts, M. Amann, N. Arnell, S. Ayeb-Karlsson, K. Belesova, H. Berry, T. Bouley, M. Boykoff, P. Byass, W. Cai, D. Campbell-Lendrum, J. Chambers, M. Daly, N. Dasandi, M. Davies, A. Depoux, P. Dominguez-Salas, P. Drummond, K.L. Ebi, P. Ekins, L.F. Montoya, H. Fischer, L. Georgeson, D. Grace, H. Graham, I. Hamilton, S. Hartinger, J. Hess, I. Kelman, G. Kiesewetter, T. Kjellstrom, D. Kniveton, B. Lemke, L. Liang, M. Lott, R. Lowe, M.O. Sewe, J. Martinez-Urtaza, M. Maslin, L. McAllister, S.J. Mikhaylov, J. Milner, M. Moradi-Lakeh, K. Morrissey, K. Murray, M. Nilsson, T. Neville, T. Oreszczyn, F. Owfi, O. Pearman, D. Pencheon, S. Pye, M. Rabbaniha, E. Robinson, J. Rocklöv, O. Saxer, S. Schütte, J.C. Semenza, J. Shumake-Guillemot, R. Steinbach, M. Tabatabaei, J. Tomei, J. Trinanes, N. Wheeler, P. Wilkinson, P. Gong, H. Montgomery, A. Costello, The 2018 report of the Lancet Countdown on health and climate change: shaping the health of nations for centuries to come, The Lancet 392 (2018) 2479–2514, https://doi.org/10.1016/S0140-6736(18)32594-7.

[13] Y. Kestens, A. Brand, M. Fournier, S. Goudreau, T. Kosatsky, M. Maloley, A. Smargiassi, Modelling the variation of land surface temperature as determinant of risk of heat-related health events, Int. J. Health Geogr. 10 (2011) 7, https://doi.org/10.1186/1476-072X-10-7.

[14] C. Buscail, E. Upegui, J.-F. Viel, Mapping heatwave health risk at the community level for public health action, Int. J. Health Geogr. 11 (2012) 38, https://doi.org/10.1186/1476-072X-11-38.

[15] L. Sun, C. Xie, Y. Qin, R. Zhou, H. Wu, S. Che, Study on temperature regulation function of green spaces at community scale in high-density urban areas and planning design strategies, Urban For. Urban Green 101 (2024) 128511, https://doi.org/10.1016/j.ufug.2024.128511.

[16] N. Wang, J. Chen, T. He, X. Xu, L. Liu, Z. Sun, Z. Qiao, D. Han, Understanding the differences in the effect of urbanization on land surface temperature and air temperature in China: insights from heatwave and non-heatwave conditions, Environ. Res. Lett. 18 (2023) 104038, https://doi.org/10.1088/1748-9326/acfc58.

[17] K.-H. Kim, E. Kabir, S. Kabir, A review on the human health impact of airborne particulate matter, Environ. Int. 74 (2015) 136–143, https://doi.org/10.1016/j.envint.2014.10.005.

[18] B.-J. He, J. Wang, J. Zhu, J. Qi, Beating the urban heat: situation, background, impacts and the way forward in China, Renew. Sustain. Energy Rev. 161 (2022) 112350, https://doi.org/10.1016/j.rser.2022.112350.

[19] Y. Wu, H. Chen, The diffusion of traffic pollutants in different residential blocks based on spatial morphological clustering, Build. Environ. 228 (2023) 109860, https://doi.org/10.1016/j.buildenv.2022.109860.

[20] L. Yao, T. Li, M. Xu, Y. Xu, How the landscape features of urban green space impact seasonal land surface temperatures at a city-block-scale: an urban heat island study in Beijing, China, Urban For. Urban Green. 52 (2020) 126704, https://doi.org/10.1016/j.ufug.2020.126704.

[21] S. Li, B. Zou, X. Ma, N. Liu, Z. Zhang, M. Xie, L. Zhi, Improving air quality through urban form optimization: a review study, Build. Environ. 243 (2023) 110685, https://doi.org/10.1016/j.buildenv.2023.110685.

[22] L. Guo, X. Guo, B. Li, E. Wang, The impact of block morphology on urban microclimates: a case study of three cities in cold regions of China, Urban Clim 57 (2024) 102098, https://doi.org/10.1016/j.uclim.2024.102098.

[23] Y. Xu, C. Ren, P. Ma, J. Ho, W. Wang, K.K.-L. Lau, H. Lin, E. Ng, Urban morphology detection and computation for urban climate research, Landsc. Urban Plan. 167 (2017) 212–224, https://doi.org/10.1016/j.landurbplan.2017.06.018.

[24] A. Zhang, W. Li, C. Xia, H. Guo, The impact of urban landscape patterns on land surface temperature at the street block level: evidence from 38 big Chinese cities, Environ. Impact Assess. Rev. 110 (2025) 107673, https://doi.org/10.1016/j.eiar.2024.107673.

[25] S. Tsoka, Investigating the relationship between urban spaces morphology and local microclimate: a study for Thessaloniki, Procedia Environ. Sci. 38 (2017) 674–681, https://doi.org/10.1016/j.proenv.2017.03.148.

[26] B.-J. He, L. Ding, D. Prasad, Enhancing urban ventilation performance through the development of precinct ventilation zones: a case study based on the Greater Sydney, Australia, Sustain. Cities Soc 47 (2019) 101472, https://doi.org/10.1016/j.scs.2019.101472.

[27] J. Hang, L. Zeng, Y. Shi, L. Ren, D. Wang, Y. Dai, X. Wang, Evaluation of surface urban energy and water balance scheme (SUEWS) using scaled 2D model experiments under various seasons and sky conditions, Urban Clim 54 (2024) 101851, https://doi.org/10.1016/j.uclim.2024.101851.

[28] M.M. Elzeni, A.A. ELMokadem, N.M. Badawy, Impact of urban morphology on pedestrians: a review of urban approaches, Cities 129 (2022) 103840, https://doi.org/10.1016/j.cities.2022.103840.

[29] Y. Wang, Z. Guo, J. Han, The relationship between urban heat island and air pollutants and them with influencing factors in the Yangtze River Delta, China, Ecol. Indic. 129 (2021) 107976, https://doi.org/10.1016/j.ecolind.2021.107976.

[30] G. Ulpiani, On the linkage between urban heat island and urban pollution island: three-decade literature review towards a conceptual framework, Sci. Total Environ. 751 (2021) 141727, https://doi.org/10.1016/j.scitotenv.2020.141727.

[31] C. Cao, X. Lee, S. Liu, N. Schultz, W. Xiao, M. Zhang, L. Zhao, Urban heat islands in China enhanced by haze pollution, Nat. Commun. 7 (2016) 12509, https://doi.org/10.1038/ncomms12509.

[32] J. Ngarambe, S.J. Joen, C.-H. Han, G.Y. Yun, Exploring the relationship between particulate matter, CO, SO2, NO2, O3 and urban heat island in Seoul, Korea, J. Hazard. Mater. 403 (2021) 123615, https://doi.org/10.1016/j.jhazmat.2020.123615.

[33] J. Zhang, Y. Wan, M. Tian, H. Li, K. Chen, X. Xu, L. Yuan, Comparing multiple machine learning models to investigate the relationship between urban morphology and PM2.5 based on mobile monitoring, Build. Environ. 248 (2024) 111032, https://doi.org/10.1016/j.buildenv.2023.111032.

[34] L. Liu, H. He, Y. Zhu, J. Liu, J. Wu, Z. Tan, H. Xie, Spatiotemporal distribution characteristics and multi-factor analysis of near-surface PM2.5 concentration in local-scale urban areas, Atmosphere (Basel) 14 (2023) 1583, https://doi.org/10.3390/atmos14101583.

[35] H. Yelixiati, L. Tong, S. Luo, Z. Chen, Spatiotemporal heterogeneity of the relationship between urban morphology and land surface temperature at a block scale, Sustain. Cities Soc. 113 (2024) 105711, https://doi.org/10.1016/j.scs.2024.105711.

[36] Y. Chen, B. Shan, X. Yu, Study on the spatial heterogeneity of urban heat islands and influencing factors, Build. Environ. 208 (2022) 108604, https://doi.org/10.1016/j.buildenv.2021.108604.

[37] J. Zhang, J. Chen, W. Zhu, Y. Ren, J. Cui, X. Jin, Impact of urban space on PM2.5 distribution: a multiscale and seasonal study in the Yangtze River Delta urban agglomeration, J. Environ. Manage. 363 (2024) 121287, https://doi.org/10.1016/j.jenvman.2024.121287.

[38] J. Yang, J. Su, X. Xia, C. Jin, X. Li, Q. Ge, The impact of spatial form of urban architecture on the Urban thermal environment: a case study of the Zhongshan district, Dalian, China, IEEE J. Sel. Top. Appl. Earth Obs. Remote Sens. 11 (2018) 2709–2716, https://doi.org/10.1109/JSTARS.2018.2808469.

[39] J. Li, C. Song, L. Cao, F. Zhu, X. Meng, J. Wu, Impacts of landscape structure on surface urban heat islands: a case study of Shanghai, China, Remote Sens. Environ. 115 (2011) 3249–3263, https://doi.org/10.1016/j.rse.2011.07.008.

[40] D. Jareemit, J. Liu, M. Srivanit, Modeling the effects of urban form on ventilation patterns and traffic-related PM2.5 pollution in a central business area of Bangkok, Build. Environ. 244 (2023) 110756, https://doi.org/10.1016/j.buildenv.2023.110756.

[41] Z. Zhu, Y. Shen, W. Fu, D. Zheng, P. Huang, J. Li, Y. Lan, Z. Chen, Q. Liu, X. Xu, X. Yao, How does 2D and 3D of urban morphology affect the seasonal land surface temperature in Island City? A block-scale perspective, Ecol. Indic. 150 (2023) 110221, https://doi.org/10.1016/j.ecolind.2023.110221.

[42] J. Yang, Y. Yang, D. Sun, C. Jin, X. Xiao, Influence of urban morphological characteristics on thermal environment, Sustain. Cities Soc. 72 (2021) 103045, https://doi.org/10.1016/j.scs.2021.103045.

[43] Z. Liang, J. Huang, Y. Wang, F. Wei, S. Wu, H. Jiang, X. Zhang, S. Li, The mediating effect of air pollution in the impacts of urban form on nighttime urban heat island intensity, Sustain. Cities Soc. 74 (2021) 102985, https://doi.org/10.1016/j.scs.2021.102985.

[44] W. Cao, W. Zhou, W. Yu, T. Wu, Combined effects of urban forests on land surface temperature and PM2.5 pollution in the winter and summer, Sustain. Cities Soc. 104 (2024) 105309, https://doi.org/10.1016/j.scs.2024.105309.

[45] Z. Lin, H. Xu, X. Hu, Z. Liu, X. Yao, Z. Zhu, Characterizing the seasonal relationships between urban heat island and surface energy balance fluxes considering the impact of three-dimensional urban morphology, Build. Environ. 265 (2024) 112017, https://doi.org/10.1016/j.buildenv.2024.112017.

[46] A. Zhang, C. Xia, W. Li, Relationships between 3D urban form and ground-level fine particulate matter at street block level: evidence from fifteen metropolises in China, Build. Environ. 211 (2022) 108745, https://doi.org/10.1016/j.buildenv.2021.108745.

[47] Y. Wu, H. Chen, Optimizing block morphology for reducing traffic pollutant concentration in adjacent external spaces of street canyons: a machine learning approach, Build. Environ. 242 (2023) 110587, https://doi.org/10.1016/j.buildenv.2023.110587.

[48] J. Xu, M. Liu, Y. Chao, H. Chen, A novel prediction framework for estimating high spatial resolution near-ground PM2.5 and O3 concentrations at street-level in urban areas, Build. Environ. 267 (2025) 112141, https://doi.org/10.1016/j.buildenv.2024.112141.

[49] L. Wang, A.P.K. Tai, C.-Y. Tam, M. Sadiq, P. Wang, K.K.W. Cheung, Impacts of future land use and land cover change on mid-21st-century surface ozone air quality: distinguishing between the biogeophysical and biogeochemical effects, Atmospheric Chem. Phys. 20 (2020) 11349–11369, https://doi.org/10.5194/acp-20-11349-2020.

[50] M. Hatzopoulou, M.F. Valois, I. Levy, C. Mihele, G. Lu, S. Bagg, L. Minet, J. Brook, Robustness of land-use regression models developed from mobile air pollutant measurements, Environ. Sci. Technol. 51 (2017) 3938–3947, https://doi.org/10.1021/acs.est.7b00366.

[51] L. Han, J. Zhao, Y. Gao, Z. Gu, Prediction and evaluation of spatial distributions of ozone and urban heat island using a machine learning modified land use regression method, Sustain. Cities Soc. 78 (2022) 103643, https://doi.org/10.1016/j.scs.2021.103643.

[52] L. Han, J. Zhao, Y. Gao, Z. Gu, K. Xin, J. Zhang, Spatial distribution characteristics of PM2.5 and PM10 in Xi'an City predicted by land use regression models, Sustain. Cities Soc. 61 (2020) 102329, https://doi.org/10.1016/j.scs.2020.102329.

[53] B.T. Dinkelacker, P. Garcia Rivera, J.D. Marshall, P.J. Adams, S.N. Pandis, High-resolution downscaling of source resolved PM2.5 predictions using machine learning models, Atmos. Environ. 310 (2023) 119967, https://doi.org/10.1016/j.atmosenv.2023.119967.

[54] D.J. Henderson, S.C. Kumbhakar, C.F. Parmeter, A simple method to visualize results in nonlinear regression models, Econ. Lett. 117 (2012) 578–581, https://doi.org/10.1016/j.econlet.2012.07.040.

[55] K.J. Preacher, A.F. Hayes, Asymptotic and resampling strategies for assessing and comparing indirect effects in multiple mediator models, Behav. Res. Methods 40 (2008) 879–891, https://doi.org/10.3758/BRM.40.3.879.

[56] Z. Qian, Hangzhou, Cities 48 (2015) 42–54, https://doi.org/10.1016/j.cities.2015.06.004.

[57] X. He, W. Gao, R. Wang, Effect of urban structure on land surface temperature around elementary schools in Hangzhou based on local climate zones, Sustain. Cities Soc. 114 (2024) 105724, https://doi.org/10.1016/j.scs.2024.105724.

[58] W. Wang, H. Chen, Y. Lai, Modeling airflow dynamics and their effects on PM2.5 concentrations in urban ventilation corridors of Hangzhou, Sci. Total Environ. 957 (2024) 177794, https://doi.org/10.1016/j.scitotenv.2024.177794.

[59] X. Zhong, L. Zhao, P. Ren, X. Zhang, C. Luo, Y. Li, J. Wang, Downscaled high spatial resolution images from automated machine learning for assessment of urban structure effects on land surface temperatures, Build. Environ. 264 (2024) 111934, https://doi.org/10.1016/j.buildenv.2024.111934.

[60] M.K. Firozjaei, N. Mijani, M. Kiavarz, S.-B. Duan, P.M. Atkinson, S.K. Alavipanah, A novel surface energy balance-based approach to land surface temperature downscaling, Remote Sens. Environ. 305 (2024) 114087, https://doi.org/10.1016/j.rse.2024.114087.

[61] J.C. Price, Estimating surface temperatures from satellite thermal infrared data—A simple formulation for the atmospheric effect, Remote Sens. Environ. 13 (1983) 353–361, https://doi.org/10.1016/0034-4257(83)90036-6.

[62] A. Sekertekin, Validation of physical radiative transfer equation-based land surface temperature using landsat 8 satellite imagery and SURFRAD in-situ measurements, J. Atmospheric Sol.-Terr. Phys. 196 (2019) 105161, https://doi.org/10.1016/j.jastp.2019.105161.

[63] K. Mao, Z. Qin, J. Shi, P. Gong, A practical split-window algorithm for retrieving land-surface temperature from MODIS data, Int. J. Remote Sens. (2005), https://doi.org/10.1080/01431160500044713.

[64] P. Dash, F.-M. Göttsche, F.-S. Olesen, H. Fischer, Retrieval of land surface temperature and emissivity from satellite data: physics, theoretical limitations and current methods, J. Indian Soc. Remote Sens. 29 (2001) 23–30, https://doi.org/10.1007/BF02989910.

[65] Y. Fang, L. Zhao, B. Dou, Y. Li, S. Wang, Circuit VRC: A circuit theory-based ventilation corridor model for mitigating the urban heat islands, Build. Environ. 244 (2023) 110786, https://doi.org/10.1016/j.buildenv.2023.110786.

[66] K.J. Preacher, D.D. Rucker, A.F. Hayes, Addressing moderated mediation hypotheses: theory, methods, and prescriptions, Multivar. Behav. Res. (2007), https://doi.org/10.1080/00273170701341316.

[67] L. Li, S. Dingyi, L. Xiaofang, J. Zhide, Influence of peasant household differentiation and risk perception on soil and water conservation tillage technology adoption- an analysis of moderating effects based on government subsidies, J. Clean. Prod. 288 (2021) 125092, https://doi.org/10.1016/j.jclepro.2020.125092.

[68] Z. Zhang, S. Tan, W. Tang, A GIS-based spatial analysis of housing price and road density in proximity to urban lakes in Wuhan City, China, Chin. Geogr. Sci. 25 (2015) 775–790, https://doi.org/10.1007/s11769-015-0788-4.

[69] W. Shen, Q. Hu, Z. Zhang, L. Niu, Comprehending the interaction between urban function and morphology at traffic analysis zones scale: the case study from Hangzhou, Geogr. J. (2025) e12620, https://doi.org/10.1111/geoj.12620 n/a.

[70] X. Dai, Z. Li, L. Ma, J. Jin, The spatio-temporal pattern and spatial effect of installation of lifts in old residential buildings: evidence from Hangzhou in China, Land (Basel) 11 (2022) 1600, https://doi.org/10.3390/land11091600.

[71] W. Wang, J. He, X. Wang, Quantitatively comparing the morphological influences on the cool island effect in urban waterfront blue-green spaces across six cities near 30°N, Urban Clim. 56 (2024) 102076. https://doi.org/10.1016/j.uclim.2024.102076.

[72] C. Yang, W. Zhu, J. Sun, X. Xu, R. Wang, Y. Lu, S. Zhang, W. Zhou, Assessing the effects of 2D/3D urban morphology on the 3D urban thermal environment by using multi-source remote sensing data and UAV measurements: a case study of the snow-climate city of Changchun, China, J. Clean. Prod. 321 (2021) 128956, https://doi.org/10.1016/j.jclepro.2021.128956.

[73] H. Bc, C. Rg, Climate downscaling: techniques and application, Clim. Res. 07 (1996) 85–95, https://doi.org/10.3354/cr007085.

[74] S. Li, C. Xu, M. Su, W. Lu, Q. Chen, Q. Huang, Y. Teng, Downscaling of environmental indicators: a review, Sci. Total Environ. 916 (2024) 170251, https://doi.org/10.1016/j.scitotenv.2024.170251.

[75] E. Fahmy, D. Gordon, D. Patsios, Predicting fuel poverty at a small-area level in England, Energy Policy 39 (2011) 4370–4377, https://doi.org/10.1016/j.enpol.2011.04.057.

[76] S. Bonafoni, Downscaling of landsat and MODIS land surface temperature over the heterogeneous urban area of Milan, IEEE J. Sel. Top. Appl. Earth Obs. Remote Sens. 9 (2016) 2019–2027, https://doi.org/10.1109/JSTARS.2016.2514367.

[77] S.-B. Duan, Z.-L. Li, Spatial downscaling of MODIS land surface temperatures using geographically weighted regression: case study in Northern China, IEEE Trans. Geosci. Remote Sens. 54 (2016) 6458–6469, https://doi.org/10.1109/TGRS.2016.2585198.

[78] J. Wu, J. Li, J. Peng, W. Li, G. Xu, C. Dong, Applying land use regression model to estimate spatial variation of PM2.5 in Beijing, China, Environ. Sci. Pollut. Res. 22 (2015) 7045–7061, https://doi.org/10.1007/s11356-014-3893-5.

[79] C. Hu, H. Zeng, Decoding spatial patterns of urban thermal comfort: explainable machine learning reveals drivers of thermal perception, Environ. Impact Assess. Rev. 114 (2025) 107895, https://doi.org/10.1016/j.eiar.2025.107895.

[80] X. Chen, F. Wei, Reducing PM2.5 and O3 through optimizing urban ecological land form based on its size thresholds, Atmospheric Pollut. Res. 16 (2025) 102466, https://doi.org/10.1016/j.apr.2025.102466.

[81] Z. Zhang, W. Luan, J. Yang, A. Guo, M. Su, C. Tian, The influences of 2D/3D urban morphology on land surface temperature at the block scale in Chinese megacities, Urban Clim 49 (2023) 101553, https://doi.org/10.1016/j.uclim.2023.101553.

[82] H. Allahyari, E. Salehi, L. Zebardast, M. Fossa, H. Jafari, Simulating the impact of natural and built environment morphology on wind and NO2 concentration caused by traffic in urban valleys, Environ. Dev. Sustain. (2023), https://doi.org/10.1007/s10668-023-04204-x.

[83] J. Zou, J. Sun, A. Ding, M. Wang, W. Guo, C. Fu, Observation-based estimation of aerosol-induced reduction of planetary boundary layer height, Adv. Atmospheric Sci. 34 (2017) 1057–1068, https://doi.org/10.1007/s00376-016-6259-8.

[84] Z. Song, R. Li, R. Qiu, S. Liu, C. Tan, Q. Li, W. Ge, X. Han, X. Tang, W. Shi, L. Song, W. Yu, H. Yang, M. Ma, Global land surface temperature influenced by vegetation cover and PM2.5 from 2001 to 2016, Remote Sens. 10 (2018) 2034, https://doi.org/10.3390/rs10122034.

[85] X. Tan, X. Sun, C. Huang, Y. Yuan, D. Hou, Comparison of cooling effect between green space and water body, Sustain. Cities Soc. 67 (2021) 102711, https://doi.org/10.1016/j.scs.2021.102711.

[86] J. Fallmann, R. Forkel, S. Emeis, Secondary effects of urban heat island mitigation measures on air quality, Atmos. Environ. 125 (2016) 199–211, https://doi.org/10.1016/j.atmosenv.2015.10.094.

[87] H. Li, F. Meier, X. Lee, T. Chakraborty, J. Liu, M. Schaap, S. Sodoudi, Interaction between urban heat island and urban pollution island during summer in Berlin, Sci. Total Environ. 636 (2018) 818–828, https://doi.org/10.1016/j.scitotenv.2018.04.254.

[88] M.E. Poli, C. Distefano, M. Grillo, E. Romano, Danni da Conigli Nell'Area del Giardino Botanico "Nuova Gussonea" Dell'Etna, Plant Biosyst. (1994), https://doi.org/10.1080/11263509409437229.

[89] Y. Rudich, N.M. Donahue, T.F. Mentel, Aging of organic aerosol: bridging the gap between laboratory and field studies, Annu. Rev. Phys. Chem. 58 (2007) 321–352, https://doi.org/10.1146/annurev.physchem.58.032806.104432.

[90] B. Yuan, L. Zhou, F. Hu, C. Wei, Effects of 2D/3D urban morphology on land surface temperature: contribution, response, and interaction, Urban Clim. 53 (2024) 101791, https://doi.org/10.1016/j.uclim.2023.101791.

[91] Y. Liu, W. Zhang, W. Liu, Z. Tan, S. Hu, Z. Ao, J. Li, H. Xing, Exploring the seasonal effects of urban morphology on land surface temperature in urban functional zones, Sustain. Cities Soc. 103 (2024) 105268, https://doi.org/10.1016/j.scs.2024.105268.

[92] J. Zhao, F. Guo, H. Zhang, J. Dong, Mechanisms of non-stationary influence of urban form on the diurnal thermal environment based on machine learning and MGWR analysis, Sustain. Cities Soc. 101 (2024) 105194, https://doi.org/10.1016/j.scs.2024.105194.

[93] J. Xu, M. Liu, H. Chen, Spatial heterogeneity of river effects on PM2.5 pollutants in waterfront neighborhoods based on mobile monitoring, Atmospheric Pollut. Res. 13 (2022) 101539, https://doi.org/10.1016/j.apr.2022.101539.

[94] L. Liu, J. Wu, Z. Liang, J. Gao, J. Hang, J. Liu, L. Liu, Spatio-temporal analysis of local thermal environment in waterfront blocks along the both sides of pearl river in Guangzhou, China, Case stud, Therm. Eng. 53 (2024) 103875, https://doi.org/10.1016/j.csite.2023.103875.

[95] E.T. Crosman, J.D. Horel, Winter Lake breezes near the Great Salt Lake, bound.-layer meteorol. 159 (2016) 439–464. https://doi.org/10.1007/s10546-015-0117-6.

[96] W. Wang, D. Wang, H. Chen, B. Wang, X. Chen, Identifying urban ventilation corridors through quantitative analysis of ventilation potential and wind characteristics, Build. Environ. 214 (2022) 108943, https://doi.org/10.1016/j.buildenv.2022.108943.

[97] X. Chen, F. Wei, Impact of territorial spatial landscape pattern on PM2.5 and O3 concentrations in the Yangtze River delta urban agglomeration: exploration and planning strategies, J. Clean. Prod. 452 (2024) 142172, https://doi.org/10.1016/j.jclepro.2024.142172.